THE JOURNAL OF PHYSICAL CHEMISTRY B
A JOURNAL OF THE AMERICAN CHEMICAL SOCIETY

pubs.acs.org/JPCB

Article

Frequency-Domain Spectroscopic Study of the Photosystem I Supercomplexes, Isolated IsiA Monomers, and the Intact IsiA Ring

Tonu Reinot, Anton Khmelnitskiy, Valter Zazubovich, Hila Toporik, Yuval Mazor, and Ryszard Jankowiak*

Cite This: *J. Phys. Chem. B* 2022, 126, 6891−6910

Read Online

ACCESS | Metrics & More | Article Recommendations | Supporting Information

ABSTRACT: The PSI_3−$IsiA_{18}$ supercomplex is one of the largest and most complicated assemblies in photosynthesis. The IsiA ring, composed of 18 IsiA monomers ($IsiA_{18}$) surrounding the PSI trimer (PSI_3), forms under iron-deficient conditions in cyanobacteria and acts as a peripheral antenna. Based on the supercomplex structure recently determined via cryo-EM imaging, we model various optical spectra of the IsiA monomers and $IsiA_{18}$ ring. Comparison of the absorption and emission spectra of the isolated IsiA monomers and the full ring reveals that about 2.7 chlorophylls (Chls) are lost in the isolated IsiA monomers. The best fits for isolated monomers spectra are obtained assuming the absence of Chl 508 and Chl 517 and 70% loss of Chl 511. The best model describing all three hexamers and the entire ring suggests that the lowest energy pigments are Chls 511, 514, and 517. Based on the modeling results presented in this work, we conclude that there are most likely three entry points for EET from the $IsiA_6$ hexamer to the PSI core monomer, with two of these entry points likely being located next to each other (i.e., nine entry points from $IsiA_{18}$ to the PSI_3 trimer). Finally, we show that excitation energy transfer inside individual monomers is fast (<2 ps at T = 5 K) and at least 20 times faster than intermonomer energy transfer.

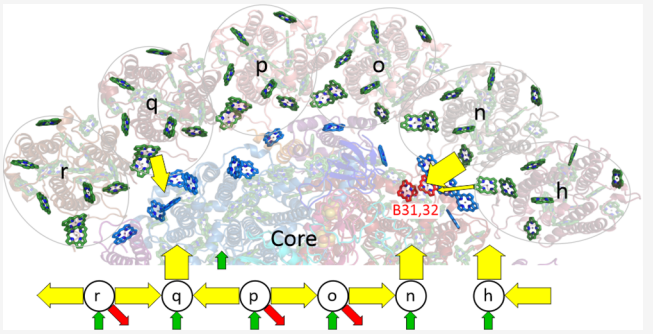

1. INTRODUCTION

Photosynthetic organisms have a remarkable ability to convert light energy into chemical energy. Two large pigment−protein complexes called Photosystem I (PSI) and Photosystem II (PSII) catalyze light-induced charge separation in photosynthetic membranes.[1] Subsequent electron transfer reactions are mediated by cofactors coordinated by both photosystems.[2] The PSI complex contains three iron−sulfur clusters as part of its internal electron transport chain and is therefore one of the main iron sinks in photosynthetic cells.

Cyanobacteria, present in almost every conceivable environment, account for more than half of the total photosynthetic productivity on Earth, including most marine and freshwater habitats.[3−5] One of the main reasons that cyanobacteria have become so ubiquitous is that their strong and effective regulatory mechanisms maintain high photosynthetic production levels under various conditions of illumination or nutrient stress.[6] Photosynthetic organisms evolved different strategies to adapt their photosynthetic apparatuses to various conditions. Adaptation to low-iron environments is an important example as iron is a common limiting factor for the growth of cyanobacteria and a wide range of adaptation mechanisms evolved to facilitate iron-limited growth.[7,8]

Under standard laboratory conditions (high concentration of iron, BG-11 medium) PSI exists as a trimer (PSI_3) in the thylakoid membranes of cyanobacteria. When cells grow under iron-deficient conditions, the cyanobacterial phycobiliprotein, PSI and PSII contents are reduced.[9] Early studies on the growth of cyanobacteria in low iron conditions revealed a remarkable adaptation of the photosynthetic membranes manifested as the induction of a chlorophyll (Chl) containing membrane antenna,[9] known also as iron-starvation induced protein A (IsiA).[10] The highly abundant chlorophyll−protein complex of iron-deficient *Synechococcus* sp. PCC7942 (CP43′) is encoded by the IsiA gene.[11]

Once IsiA is induced in cyanobacteria, it forms a large supercomplex consisting of the 18mer IsiA ring ($IsiA_{18}$) surrounding the PSI trimer.[12−14] The IsiA protein is similar to PsbC, the CP43 protein of the core of PSII, the water-splitting and oxygen-evolving enzyme of photosynthesis. Therefore, the IsiA monomer is often called CP43′.[10,11,15−17]

The spectroscopic properties of the isolated (purified) IsiA complexes are similar to those of the related CP43 complex

Received: July 8, 2022
Revised: August 9, 2022
Published: September 5, 2022

https://doi.org/10.1021/acs.jpcb.2c04829
J. Phys. Chem. B 2022, 126, 6891−6910

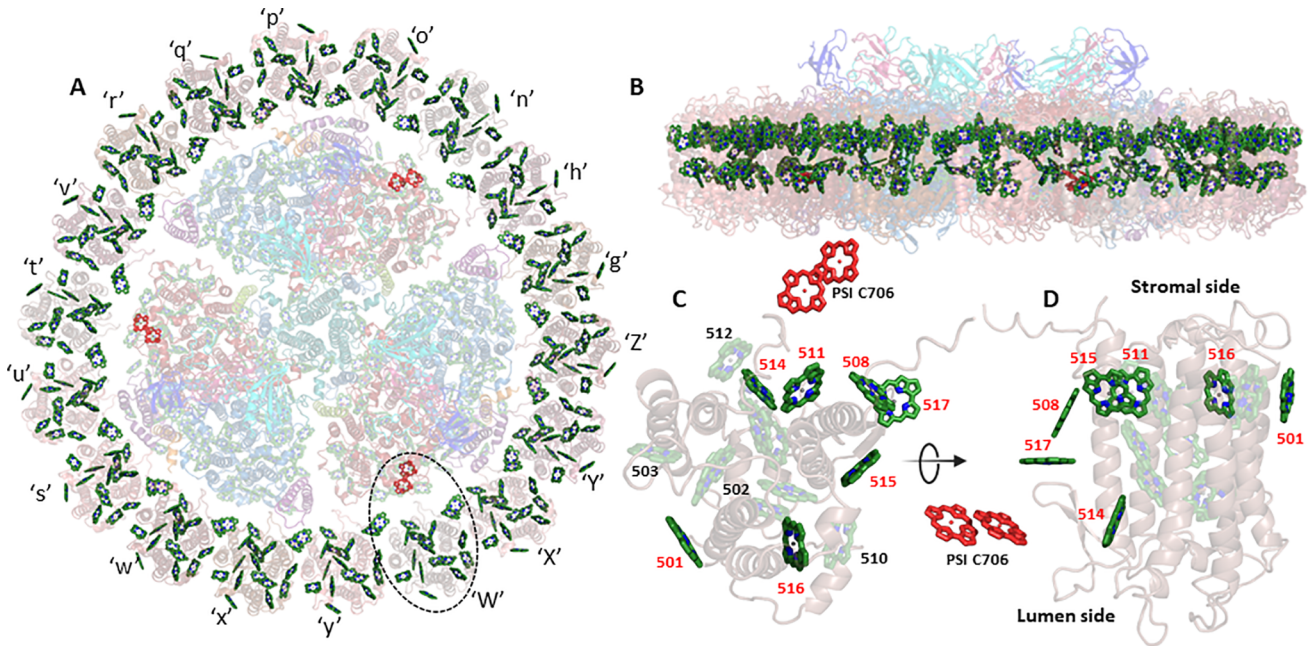

Figure 1. (A) View from the lumen side of the membrane showing the overall structure of the PSI_3–$IsiA_{18}$ supercomplex of *Synechocystis*. The trimeric PSI_3 is surrounded by a ring consisting of 18 IsiA monomers (labeled with letters "n", "o", ..., "h").[12] The PSI subunits are transparent to clearly show relevant red-absorbing pigments. This figure shows only IsiA Chls in green and the PSI C706 trap in red. C706 is one of the low-energy traps in each PSI monomer assigned to B31–B32 Chls)[25] (B) View on the structure from the membrane plane. (C) Closer view on the IsiA monomer "W" encircled in dashed line in "A". Selected Chls of interest to this work are labeled using the nomenclature of ref 12. (D) View from the membrane plane on IsiA monomer "W" showing C706 at the luminal side of the complex.

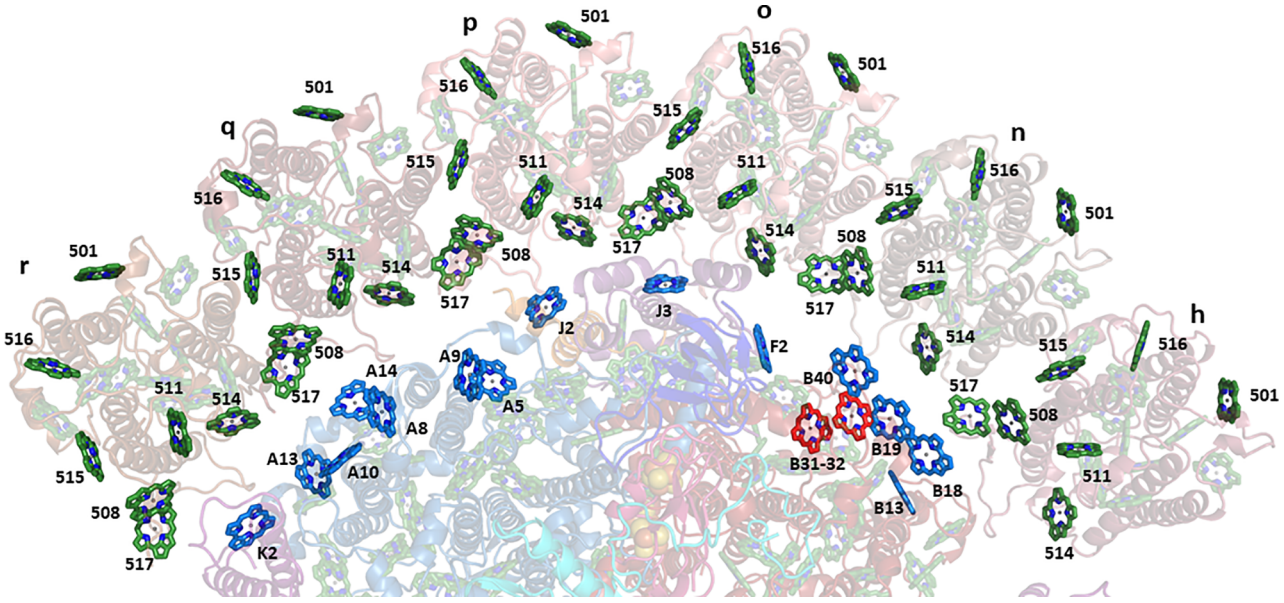

Figure 2. Structure of the IsiA hexamer. Chls likely contributing to the lowest energy state(s) in IsiA monomers are shown in green. Below the hexamer, a part of the PSI monomer is shown, emphasizing Chls at the interface between the ring and PSI monomer (in blue). The red Chls correspond to the B31–32 Chls constituting the C706 low energy trap.[25]

from plants (with 13 Chls per complex), except that the characteristic narrow absorption band of CP43 near 683 nm is weak[18] or missing in isolated IsiA.[15] This clearly indicates that some chlorophylls may be lost during isolation/purification procedures. It was recently determined that each IsiA subunit in cyanobacteria binds four additional pigments in addition to the 13 Chls observed in CP43 complex of PSII.[12] The four additional Chls contribute to the interfaces between neighboring IsiA subunits and the $IsiA_{18}$–PSI_3 interface.[12] The increase in the number of pigments associated with each reaction center allow cells to maintain their photosynthetic rates while synthesizing lower amounts of PSI_3, thereby reducing the total cellular iron consumption.[15,17,19,20] The assembly of PSI_3–$IsiA_{18}$ supercomplex seems especially robust and can also take place around PSI_3 mutants and monomers.[21,22] The Cryo-EM structure of PSI_3–$IsiA_{18}$ supercomplex of the *Synechocystis* 6803 was solved at a resolution of 3.3 Å.[12] Recently, Cao et al.[23] solved the single

https://doi.org/10.1021/acs.jpcb.2c04829
J. Phys. Chem. B 2022, 126, 6891–6910

particle structure of both PSI_3−$IsiA_{18}$−Fld (where Fld is flavodoxin and replaces the iron-containing ferredoxin (Fd) as the electron receptor of PSI) and PSI_3−$IsiA_{18}$ supercomplexes from a mesophilic cyanobacterium *Synechococcus* sp. PCC 7942 at resolutions of 3.3 and 2.9 Å, respectively. The structure of PSI_3−$IsiA_{18}$ from thermophilic cyanobacterium *Thermosynechococcus vulcanus* is also known.[24]

The overall structure of the PSI_3−$IsiA_{18}$ supercomplex is shown in Figure 1. The configuration of the different IsiA monomers around PSI_3 is flexible to some extent, and therefore, different IsiA subunits relate to each other somewhat differently across the entire ring.[12] In other words, in the first approximation, the IsiA ring has C_3 rather than C_{18} symmetry.

The ring around PSI_3 acts as a peripheral antenna; in addition to its function as energy collector, the $IsiA_{18}$ ring may also act as an energy dissipater that protects photosystems from being damaged by excess excitation energy[26,27] and helps to protect cyanobacterial cells from oxidative damage.[28] Spectroscopic investigations confirmed that the $IsiA_{18}$ antenna in the PSI_3−$IsiA_{18}$ supercomplex is tightly coupled to the core antenna of PSI_3.[17,29] Several groups engaged in studying energy transfer dynamics in $IsiA_{18}$ and PSI_3−$IsiA_{18}$ supercomplexes of cyanobacteria.[15,17,29] These works agree that the $IsiA_{18}$ ring effectively transfers energy to the PSI_3 core, although an increase of total trapping time (compared to isolated PSI_3 cores) was also observed.[17,29] Components with characteristic times from 1.7 to 10 ps observed in the *Synechocystis* supercomplexes at room temperature have been ascribed to the $IsiA_{18}$ → PSI_3 core excitation energy transfer (EET).[17] The 1.7 ps component was assigned to the fastest EET through closely located chlorophylls at the interface between the $IsiA_{18}$ and the PSI_3 core, while the 10 ps process was assigned to the overall excitation transfer from $IsiA_{18}$ to PSI_3 core.[17] Earlier analysis of the low-temperature absorption spectra of PSI_3, PSI_3−$IsiA_{18}$, and IsiA complexes suggested that there are just 13 chlorophylls (Chls) per IsiA monomer,[30] i.e., a number that was observed in the CP43 complex of Photosystem II (PSII).[31] This was in contrast with the modeling studies of Zhang et al.,[32] which suggested that IsiA likely contains 15 Chls. However, as mentioned above, the recently solved cryo-EM structures of the complex revealed 17 Chls per IsiA monomer.[12,23,24] This indicates that some pigments could be lost during isolation/purification procedures. Figure 2 shows the structure of six neighboring monomers, r, q, p, o, n, and h, and labels several pigments that could contribute to the lowest energy state(s) in each monomer.

Our previous modeling studies of various optical spectra of the isolated IsiA, using the uncorrelated EET model,[30] suggested that IsiA monomers (by analogy with the CP43 complexes of PSII core in spinach) possess two quasi-degenerate low-energy states, A′ and B′. In that case, however, the modeling was based on the available CP43 structure of PSII core complex,[33] which has smaller number of Chls. Nevertheless, it was suggested that pigments mostly contributing to the lowest-energy A′ and B′ states of the PSI_3−$IsiA_{18}$ supercomplex in *Synechocystis* are likely located on the side of the IsiA complex facing the PSI_3 core, a finding that contradicted the model of Zhang et al.,[32] but was in agreement with the model suggested by Nield et al.[33] Both the latter model and the one discussed in ref 30 are consistent with the recent Cryo-EM structure.[12] However, identification of pigments contributing to the lowest energy state(s) of IsiA monomers is still controversial, as the spectra reported in the literature vary from laboratory to laboratory and modeling was based on the CP43 structure and not the CP43′ (i.e., IsiA complex) one. Below, we discuss various types of new low-temperature spectra, including hole-burned (HB) spectra, obtained recently for the PSI_3−$IsiA_{18}$ sample and isolated IsiA monomer (IsiA) complexes of *Synechocystis* 6803. In this work, modeling of experimental data is based on the recently determined cryo-EM supercomplex structure.[12] Two hexamer models ($IsiA_6$) and two matching IsiA monomer models (with a different pigment composition of the low-energy states) are discussed in detail, including the excitonic structure and dynamics. For example, we suggest that isolated IsiA monomers lost 100% of Chls 501 and 517 and 70% of Chl 511 (in model *MA*). In the monomer *MB* model the missing pigments are assigned to Chls 508 and 517 while Chl 511 is also lost in 70% of the complexes. In the hexamer models, i.e. *HexA* and *HexB*, all 17 pigments are present in each monomers of the ring; in these two models, the lowest energy pigments are assigned to Chls (514, 511, 501) and (514, 511, 517), respectively. We argue that only model (for monomers), model *HexB* (for hexamers) and model *HexB* for the entire ring $IsiA_{18}$ are consistent with experimental data. We also show that excitation energy transfer within individual IsiA monomers is fast (less than 2 ps) and faster than intermonomer transfer, except for intermonomer transfer between Chls 517 and Chls 514 located on adjacent monomers. The intermonomer EET (between Chls 517 and 514 on neighboring monomers) is about 0.5 ps, and there are likely three entry points per PSI core monomer for the ring-core EET in our samples, though two entry points cannot be entirely excluded.

2. MATERIALS AND METHODS

2.1. Preparation of PSI_3−$IsiA_{18}$ Supercomplex and Isolated IsiA Monomer. *Synechocystis PCC*6803 cyanobacteria were cultured in glass bottles in 10-L batches using BG11 medium supplemented with 12 ng/mL ferric ammonium citrate and 5 mM glucose in 30 °C and bubbled with air. Light was supplied from an LED array (Fluence RAY) at very low intensities (∼15 μE). PSI_3−$IsiA_{18}$ supercomplexes were isolated as described in ref 12. Here, 20−40 L of culture was harvested using centrifugation and washed once with STN1 buffer (30 mM Tricine-NaOH pH 8, 15 mM NaCl, 0.4 M sucrose). Cells were resuspended in STN1 and broken with two cycles at 30 KPSI in a cell disruptor (Constant Systems Ltd.). The lysate was cleared by centrifugation in a F20-12X50 LEX rotor for 10 min at 12000 rpm in Sorval LYNX 6000 centrifuge (Thermo Scientific). Membranes in the supernatant were pelleted using ultracentrifugation (Ti70 rotor, 45000 rpm for 2 h) and resuspended in STN2 (30 mM Tricine-NaOH pH-8, 100 mM NaCl, 0.4 M sucrose). After resuspension in STN2, the membranes were incubated on ice for 30 min, then collected again (Ti70 rotor, 45000 rpm, 2 h) and resuspended in STN1. *n*-Dodecyl β-D-maltoside (DDM, Glycon) was added to the membranes at a 10:1 DDM to chlorophyll ratio. The suspension was gently mixed by hand a few times then incubated on ice for 30 min. After solubilization, the insoluble material was discarded using ultracentrifugation (Ti70, 45000 rpm, 30 min). The solubilized membranes were loaded onto a DEAE column (Toyopearl DEAE-650C). The complexes were eluted using a linear NaCl gradient (15−500 mM NaCl) in 30 mM Tricine−NaOH pH 8, 0.2% DDM. Dark green fractions were collected and precipitated using 6% PEG3350 (Hampton

https://doi.org/10.1021/acs.jpcb.2c04829
J. Phys. Chem. B 2022, 126, 6891−6910

Research). After centrifugation in a F20-12X50 LEX rotor for 5 min at 5000 rpm, the green precipitate was resuspended in 30 mM Tricine−NaOH pH 8, 75 mM NaCl with 0.05% DM and loaded onto a 12−60% sucrose density gradient, prepared with the same buffer. Following centrifugation (Beckman SW40 rotor, 37000 rpm, 16 h) the appropriate green band was precipitated using 10% PEG3350 (Hampton Research). After centrifugation in an Eppendorf tabletop for 5 min at 10000 rpm, the green precipitate was resuspended in 30 mM Tricine-NaOH pH 8, 75 mM NaCl with 0.05% DM and loaded onto a 12−60% sucrose density gradient, prepared with the same buffer. Following centrifugation (Beckman SW60 rotor, 56 000 rpm, 4 h) the green band corresponding to the $IsiA_{18}$−PSI_3 supercomplex was collected and used for subsequent experiments. The upper band corresponding to monomeric IsiA was isolated from the sucrose gradient and loaded onto DEAE column and eluted with 30 mM Tricine−NaOH pH 8, 350 mM NaCl, and 0.05% DM. For purification details of the PSI_3−$IsiA_{18}$ complex and IsiA monomer see Figure S1 in the Supporting Information. For low-temperature experiments, samples were diluted with 1:2 (v/v) buffer:cryoprotectant solution. The glass forming cryoprotectant mixture was 55:45 (v/v) glycerol:ethylene glycol. All complexes studied in this work were most likely in their oxidized state (see Section 5.2 for more details), so there is no $P700^+$ minus P700 signal or electrochromic shifts that could affect some of the results discussed in this work.

2.2. Instrumentation. Details about the measurement setup were described elsewhere.[30] Briefly, a Bruker HR125 Fourier transform spectrometer was used to measure the absorption and hole-burned (HB) spectra with resolutions of 4 and 0.5−2 cm^{-1}, respectively. The 488.0 nm excitation for nonresonant HB (NRHB) spectra was produced by a Coherent Innova-90 argon ion laser. Spectral holes (bleaches produced by resonant excitation, see below) were obtained with a Coherent CR699 ring dye laser pumped by a Spectra-Physics Millennia Xs diode laser (532 nm). With laser dye LD 688 (Exciton), the spectral range of 650−720 nm was available with a line width of 0.07 cm^{-1}. Laser power in all experiments was precisely set by a continuously adjustable neutral density filter. Low-temperature (4 K) experiments were performed using an Oxford Instruments Optistat CF2 cryostat with sample temperature controlled by a Mercury iTC temperature controller. Fluorescence spectra were collected with a resolution of 0.1 nm at 4 K by a Princeton Instruments Acton SP-2300 spectrograph equipped with a back-illuminated CCD camera (PI ActonSpec10, 1340 × 400). The excitation source was 488.0 and/or 496.5 nm laser lines from a Coherent Innova-90 argon ion laser.

2.3. Spectroscopic Methodologies. Spectral hole burning relies on differences observed in the absorption spectrum of a low-temperature system before and after narrow-band laser excitation. If a pigment molecule (in resonance with the laser) experiences a photochemical reaction, it ceases to absorb at its original wavelength/frequency because it is chemically altered, and one speaks of photochemical HB (PHB). Both PHB and NPHB may result in the formation of persistent holes, meaning that holes are preserved for hours or even days after the initial excitation is turned off, as long as a low temperature is maintained. In either case, the difference between the measured absorption spectrum before and after laser excitation reveals the HB spectrum. In this work, we use NPHB; in this case, the pigment molecule does not undergo a chemical reaction, but its immediate environment experiences some rearrangement (for more details see refs 34 and 35). Persistent resonant HB spectra can unmask a zero-phonon hole (ZPH) at the frequency of the original excitation and phonon sideband (PSB); the entire shape of ZPH/PSB allows one to estimate the strength of electron−phonon (el-ph) coupling (i.e., the Huang−Rhys factor S). Generation of transient HB spectra requires the presence of a third, relatively long-lived state. That is, the excited state evolves into a triplet state or is converted (e.g., by charge transfer) to another long-lived (μs to ms range) product leaving a transient hole in the absorption spectrum.[34,36] In this case, the pigment's ground state is depopulated for the lifetime of the long-lived state, and the spectral hole will be observable only for the duration of this lifetime. The transient holes discussed in the main manuscript are acquired as the difference between the absorption spectra measured while the excitation is on and off.[34,36,37] Non-resonant holes are obtained by excitation of high-energy pigments or high-energy spectral bands.[38] In this case, radiationless EET takes place from high-energy pigment(s) to the low-energy pigment(s) or from higher energy states (excitons) to the lowest energy pigment(s) or state(s). In general, EET occurs from a manifold of vibrational states, associated with the excited electronic state of the donor molecule, into a manifold of vibrational states associated with the ground state of the acceptor molecule. (For more details on HB spectroscopy, see refs 34 and 36.)

2.4. Modeling Studies of Various Experimental Spectra for the 6NWA PDB Structure. In the present work, measured optical spectra are modeled using a second-order non-Markovian theory[39] with the Nelder−Mead simplex algorithm for parameter optimization. That is, a multidimensional unconstrained minimization is used to search the solution space and to minimize the root-mean square deviation between multiple calculated and measured bulk spectra. A calculated bulk spectrum is an average of (typically) 20 000 $IsiA_6$ hexamers (102 pigments) or 200−500 000 $IsiA_1$ monomer spectra (for a variable number of Chls, i.e., 15−17). In brief, the off-diagonal coupling matrix elements (V_{mn}) are calculated using the TrEsp method[40] based on the supercomplex structure (6NWA PDB structure)[12] with 18 IsiA monomers, each containing 17 chlorophylls. In this work, the transition charges from electrostatic potentials (TrEsp) method was used with the equation written as[40]

$$V_{mn} = \frac{f}{4\pi\varepsilon_0} \sum_{I}^{N} \sum_{J}^{N} \frac{q_I^m(1,0) q_J^n(0,1)}{|\vec{r}_I - \vec{r}_J|} \quad (1)$$

where $f = 1$ and ε_0 are screening factor and dielectric constant, respectively. For actual Chl *a* atomic charges, we used TDDFT/B3LYP values (with the constraint that partial charges for all H atoms are 0) given in Table 1 of the Supporting Information in ref 40. The excitonic couplings result from the atomic transition charges q_I^m (1,0) and q_J^n (0,1); these charges are determined for pigments *m* and *n* using a time-dependent density functional theory that fits the electrostatic potentials of the transition (or charge) densities to yield the appropriate vacuum dipole moments.[40−42] The transition dipole moments of 4.6 D for all Chls were used in our calculation. For completeness, we add that our coupling constants are calculated without hydrogen atoms and using planar Chl rings. This assumption is appropriate for a low-resolution (3.3 Å) 6NWA structure. As shown in the

https://doi.org/10.1021/acs.jpcb.2c04829
J. Phys. Chem. B 2022, 126, 6891−6910

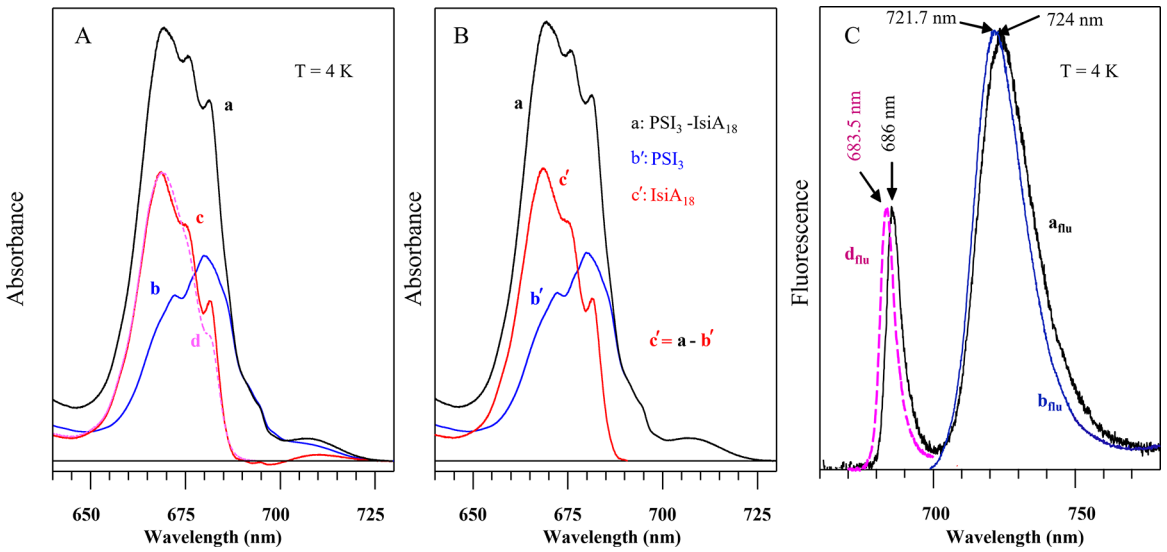

Figure 3. (A) Curves a, b, and d show the measured 4 K absorption spectra of PSI_3−$IsiA_{18}$ supercomplex, the isolated PSI_3 trimer, and isolated IsiA monomer, respectively. Absorptions of PSI_3−$IsiA_{18}$ supercomplex and the isolated PSI_3 are area-normalized according to Chl content. Curve c (red) is the difference between spectra a and b (c = a-b). (B) Spectra c′and b′ correspond to corrected ("pure") contributions assigned to PSI_3 trimer and $IsiA_{18}$ ring, respectively; see text for details. Curve a is the same as in frame A. (C) Emission spectra of PSI_3−$IsiA_{18}$ supercomplex (a_{flu}), the isolated PSI_3 trimer (b_{flu}), and isolated IsiA monomer (d_{flu}). Spectra are normalized to emissions maxima.

Supporting Information, a contribution from hydrogens and possible deviation from planarity of Chls weakly affects the V_{nm} parameters, and as a result, the site energies were obtained from simulation of multiple optical spectra. For example, depending on Chl, the calculated site energies in the presence of hydrogens and nonplanar Chl rings varied within the 0.23 to 2.9 cm^{-1} range (with the averaged standard deviation of 1.7 cm^{-1}). The average standard deviation for the calculated inhomogeneous widths was also small (about 2 cm^{-1}). Thus, below we used V_{nm} parameters obtained directly from the Cryo-EM structure of PSI_3−$IsiA_{18}$ supercomplex solved at a resolution of 3.3 Å.

Chls numbering in the different PDB models is shown in Table S1 in the Supporting Information. Static energy disorder (inhomogeneous broadening) is introduced into the diagonal matrix elements by a Monte Carlo approach with normal pigment Site Distribution Functions (SDF) centered at E_n^0 (n labeling various pigments, i.e., n = 1−17) and with fwhm representing Γ_{inh}^n, which can be site-dependent. E_n^0 values correspond to the vertical energies rather than the energies of zero-phonon transitions. Eigen-decomposition of the coupling matrix provides eigen-coefficients (E_n^M) and eigenvalues (v_M). E_n^0, Γ_{inh}^n, and phonon and vibrational Huang−Rhys factors (S) can be independent or dependent (e.g., several Γ_{inh} can have the same optimizable value) free (or fixed) parameters; all independent free parameters are optimized simultaneously against the experimental spectra. We assume that the phonon spectral density (weighted phonon profile) can be described by a continuous function, which is chosen to be a log-normal distribution used for Chls *a* in CP29 complex.[43] In all simulations, vibrational modes are dynamically localized as in ref 44. In general, a partially coherent energy relaxation is expected within IsiA monomers if pigments are strongly coupled. Our in-house software allows simultaneous calculation of a dozen different optical spectra, of which absorption, emission, circular dichroism (CD), and nonresonant HB (NRHB) spectra are relevant to this work. NRHB spectra are calculated in two stages: at first, a preburn absorption spectrum of a single pigment−protein complex is calculated. Thermally weighed and quantum-weighed occupation numbers (squared eigenvector coefficients) of the lowest energy exciton states are used to determine the most likely pigment to experience NPHB. The postburn site-energy of the burned pigment is randomly selected from the original site distribution function, whereas all other diagonal elements of the Hamiltonian are left unchanged. The Hamiltonian is again diagonalized, and a postburn absorption spectrum is calculated. The resulting single complex NRHB spectrum is calculated as the preburn absorption subtracted from the postburn absorption spectrum.

The above calculations were performed for all individual IsiA monomers and all three $IsiA_6$ hexamers to consider EET processes along the ring, as EET times between monomers are not the same. The EET rates for Chls belonging to different IsiA monomers (see Section 4.4) were calculated in Förster approximation; for details see ref 45 Briefly, ZPL-based site energies of the relevant pigments were obtained by a Monte Carlo approach, and the dependence of spectral overlap on donor−acceptor ZPL-ZPL energy gap was used to produce a distribution of EET rates (or times).[46,47] In the current work, single chromophore Förster resonance energy transfer (FRET) approach is used; in the future, particularly when higher resolution structure becomes available, one could apply the multichromophore FRET approach.[48−50] The latter, however, may ultimately be more relevant to properly describe EET from the ring to the core, but not so much within the ring, as discussed below.

3. EXPERIMENTAL RESULTS

3.1. Low-Temperature Absorption and Emission Spectra. Curves a and b in frame A of Figure 3 correspond to 4 K absorption spectra of *Synechocystis* PSI_3−$IsiA_{18}$ supercomplex (591 Chls) and isolated PSI_3 trimer (285 Chls), respectively, normalized for pigment content. For the corresponding emission spectra (labeled as a_{flu} and b_{flu} and normalized to emissions maxima), see frame C. The absorption spectrum of the supercomplex shows three maxima near 670,

https://doi.org/10.1021/acs.jpcb.2c04829
J. Phys. Chem. B 2022, 126, 6891−6910

676, and 682 nm, as well as an additional weak band near 710 nm. Spectrum c (red) in frame A is the difference between spectra a and b assigned mostly to the absorption of the $IsiA_{18}$ ring. Note that $IsiA_{18}$ absorption spectrum (c) contains a pronounced peak near 683 nm, resembling a similar narrow peak of CP43 of the PSII core,[16,51] as well as a weak band at 710 nm. However, the band near 710 nm must belong to the PSI_3 trimer. If the 710 nm band in curve c belonged to the ring absorption, each IsiA monomer would have a red-shifted trap, which is inconsistent with the significant amount of the ring emission peaked at 686 nm. A comparison of spectra a, b, and c suggests that PSI_3 residing within the supercomplex has somewhat larger oscillator strength of the low energy trap(s). This may be due to small structural differences between PSI cores in samples grown under different conditions, leading to a weaker oscillator strength of the low-energy trap(s), and blue-shifted and broader PSI_3 emission (compare the maxima in spectra a_{flu} and b_{flu} at 721.7 and 724.0 nm, respectively, in frame C). No effort was made to keep P700 in neutral/reduced state, and white light of the FTIR spectrometer was on the sample all the time. Thus, the P700 in our samples was oxidized.[52,53] Interestingly, the integrated intensity of curve c corresponds to about 309 Chls, i.e., 18 IsiA monomers with about 17.17 Chls per a single IsiA. However, for modeling study, curve c (red) in frame A must be corrected by removing the long-wavelength contributions assigned above to PSI_3; we suggest that in good approximation the corrected curve (c′ in frame B) can be assigned to the absorption intact $IsiA_{18}$ ring within the ring-core supercomplex. Thus, it is safe to assume that our sample contains about 17 Chls per IsiA monomer within the $IsiA_{18}$ ring as revealed by structural studies.[12,23] This composition is used in our ring modeling studies discussed below. Note that the absorption spectrum (curve d in frame A; dashed line) obtained for isolated IsiA monomers, in this case normalized to the maximum of curve c, is similar in shape to the spectrum c, though its lower integrated intensity suggests that some Chls are likely absent in such population (vide infra). As a result, the fluorescence spectrum of the isolated IsiA monomers (d_{flu}) shifts blue to 683.5 nm, in comparison with the 686.0 nm emission maximum observed for the intact $IsiA_{18}$ ring of the supercomplex. The blue-shifted emission in isolated IsiA monomers is also caused by the absence of EET between IsiA monomers. Note that the integral intensities of the two components of the supercomplex emission spectrum a_{flu} scale approximately as 1.0 to 4.8, which corresponds to the IsiA ring contributing about 17% of the supercomplex emission.

Regarding spectrum d_{flu}, we note that Andrizhiyevskaya et al.[15] observed a fluorescence band near 682 nm in an isolated IsiA from *Synechococcus*, while the emission band was shifted to 685 nm in their PSI_3−$IsiA_{18}$ supercomplex. These authors attributed the 682 nm → 685 nm shift to EET among the IsiA monomers, pigment−pigment interactions between the monomers, and/or interactions between the ring and PSI_3 trimer in the supercomplex. However, one cannot exclude that the observed differences in absorption and emission spectra are also affected by different number of Chls per monomer, as some Chls could be lost during isolation/purification procedures (see modeling data). The latter must lead to a different pigment composition of the lowest exciton state(s). Indeed, blue-shifted maxima near 684−685 nm (assigned to the $IsiA_{18}$ ring) were also observed in ref 18, showing sample dependent emission spectra. Spectra shown in Figure 3 are modeled and discussed in Sections 4.1 and 4.2.

3.2. Do Isolated IsiA Monomers Contain a Smaller Number of Pigments? Figure 4 shows the difference between the integrated absorption spectra of $IsiA_{18}$ ring in the Q_y-spectral region (divided by 18, i.e. assumed to represent absorption of an intact monomer residing within the ring; curve c′ from Figure 3B) and a scaled absorption of individual IsiA monomers (curve d from Figure 3A). We assume that sharp features in c′ and the difference between c′ and d are caused by missing pigments. While normalizing curve d, it was required that the subtracted curve should not contain negative vibronic absorption and that its sum vibronic Huang−Rhys factor stays similar. 2.6−2.7 missing pigments appeared to satisfy these requirements the best. That is, comparison of the integrated intensities of spectra c′ and d (i.e., c′−d) revealed that most likely about 2.6−2.7 Chls have been lost in isolated IsiA monomers. The latter is tested by the modeling study discussed below.

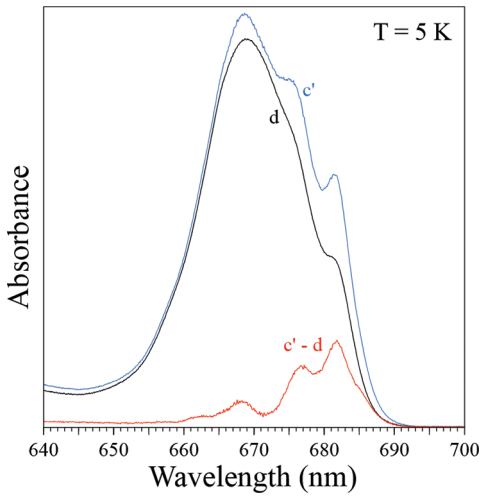

Figure 4. Curve (c′ - d) is the difference between the absorption spectra of scaled monomer absorption within the intact $IsiA_{18}$ ring (curve c′) and a typical absorption of isolated IsiA monomer (curve d).

3.3. Hole-Burned Spectra. Figure 5A shows four resonant HB spectra obtained with λ_{B1} = 683.1 nm and 2 cm^{-1} spectral resolution for the PSI_3−$IsiA_{18}$ supercomplex as a function of burning fluence. The fluences (from top to bottom in frame A) are 3.3, 16.5, 29.7, and 56.1 J/cm^2, respectively. Recall that the ZPHs are resolution limited. The inset in Figure 5A shows higher resolution (i.e., 0.5 cm^{-1}) ZPH burned at λ_{B2} = 686.0 nm with a fwhm of the ZPH of 1.2 cm^{-1}. The lowest HB spectrum (red curve in frame A), with a truncated ZPH, is also shown in frame B as curve b. The latter curve reveals that the lowest-energy trap formed via EET from $IsiA_{18}$ → PSI_3 core and EET within the PSI_3 core to the lowest-energy trap is near 709 nm. However, the lowest-energy trap for nonresonant excitation at 665.0 nm (see top blue curve in frame B) shifts red to about 712 nm. In the isolated PSI_3 trimer, this state was assigned to the so-called C714 trap of the PSI_3 core.[25] The bleaches near 692.0 and 697.5 nm belong to the PSI_3 trimer as revealed by comparison with the HB spectrum obtained at 683.1 nm for the individual IsiA monomers (compare with the lowest green curve in frame B). This is in agreement with earlier HB spectra burned in isolated PSI_3 trimer.[25] The bleach

https://doi.org/10.1021/acs.jpcb.2c04829
J. Phys. Chem. B 2022, 126, 6891−6910

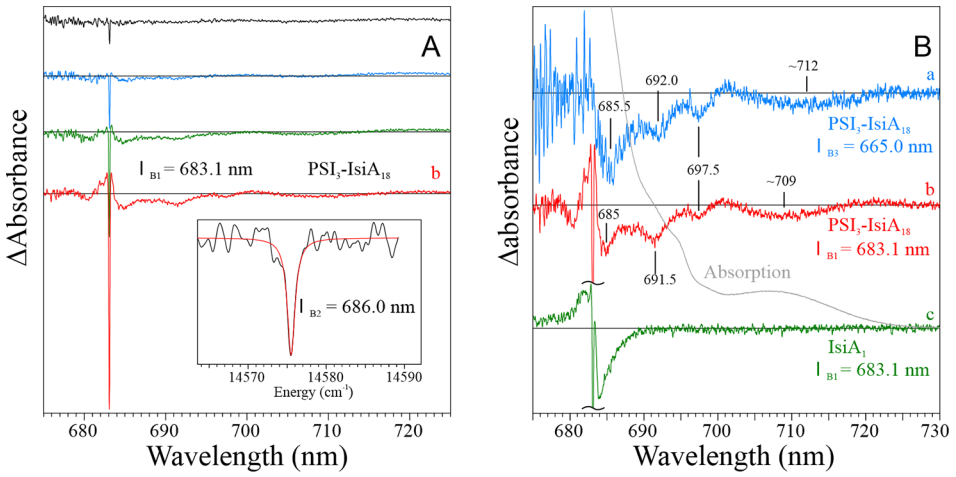

Figure 5. (A) Spectra from top to bottom are resonant HB spectra obtained at 5 K for the PSI_3–$IsiA_{18}$ supercomplex for the burning wavelength (λ_{B1}) of 683.1 nm (2 cm^{-1} resolution) as a function of fluence (see text). In this case, the ZPH width is resolution limited. The inset shows higher resolution (i.e., 0.5 cm^{-1}) ZPH burned at λ_{B2} = 686.0 nm. (B) Curves a (blue) and b (red, shown also in red in frame A) are HB spectra obtained for the PSI_3–$IsiA_{18}$ supercomplex with λ_{B3} = 665.0 and λ_{B1} = 683.1 nm, respectively. The green curve in frame B is the HB spectrum obtained for the isolated IsiA monomers (λ_{B1} = 683.1 nm). The low-energy absorption spectrum of PSI_3–$IsiA_{18}$ (gray curve) is shown for comparison.

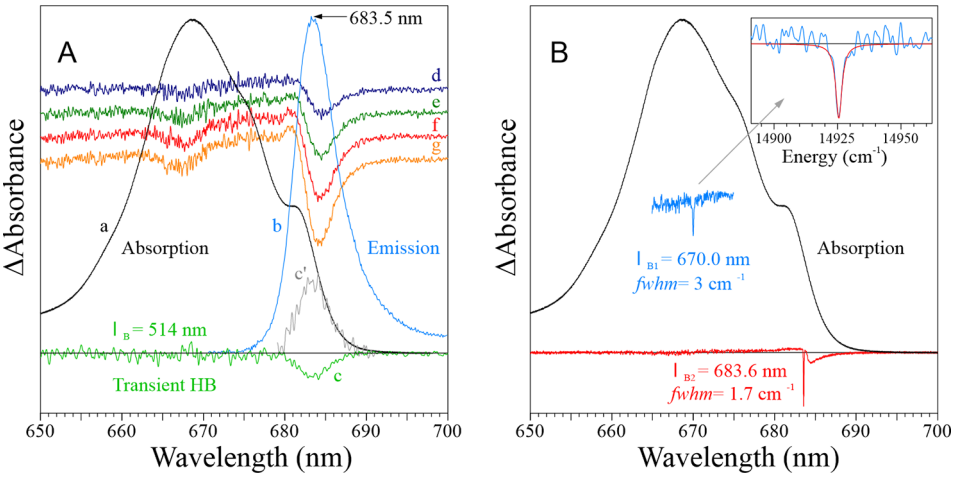

Figure 6. (A) Absorption (a) and emission (b) spectra of isolated IsiA monomer and four (persistent) nonresonant HB spectra (d–g) obtained with λ_B = 488.0 nm at T = 5 K. Spectrum c is transient nonresonant hole obtained at the same λ_B; curve c′ is expanded and inverted curve c. (B) Persistent resonant HB spectra obtained at λ_{B1} = 670.0 nm (blue) and at λ_{B2} = 683.6 nm (red curve). Black curve is the absorption spectrum. The inset shows the Lorentzian fit (red) of the ZPH burned at λ_{B1} (blue).

near 685.5 nm in curve a (Figure 5B) most likely corresponds to the lowest energy state in the $IsiA_{18}$ supercomplex. The 686 nm emission (T = 5 K; see curve a_{flu} in frame C of Figure 3) originates from the 685.5 nm state observed in curve a in Figure 5B. The origin and composition of the emission spectra are discussed in Sections 4.1 and 4.2.

Figure 6A compares transient HB spectrum (green curve c) with persistent holes (curves d–g) obtained with 488.0 nm excitation for IsiA monomer sample. Absorption and fluorescence spectra of IsiA monomers (spectra a and b, respectively) are shown for an easy comparison. Spectra d–g show clearly developed blue-shifted antiholes, which affect the high-energy side of the persistent holes. Identical transient HB spectra were obtained using 665.0 nm excitation; data not shown for brevity. Curve c′ (frame A) is the expanded and reversed transient hole (c) that illustrates the likely shape of the lowest energy bleach with a minimum at 683.2 nm (see curve c). This is consistent with resonant holes burned in IsiA monomers (see Figure 6B), which show small electron–phonon coupling strength (S) for low energy pigments; see the modeling study section for details. Persistent resonant HB spectra obtained for λ_{B1} = 670.0 nm (blue) and λ_{B2} = 683.6 nm (red), see Figure 6B, were measured using 1 cm^{-1} spectral resolution. The corresponding (resolution corrected) fwhm of these ZPHs are 3 and 1.7 cm^{-1}, respectively. The inset in Figure 6B shows the Lorentzian fit (red) of the ZPH burned at λ_{B1} = 670.0 nm. Absorption spectrum (black) is shown for comparison. Spectra a, b and c in Figure 6A are modeled in Section 4.1 (see Figure 8).

Frame A in Figure 7 shows four persistent resonant HB spectra (curves a–d) obtained for the PSI_3–$IsiA_{18}$ supercomplex with λ_B of 707.7 nm. Low-energy part of the absorption spectrum (gray line) is shown for an easy comparison. Interestingly, in contrast to HB spectra produced with burning at the same wavelength in the isolated PSI_3 trimer of wild-type (WT) PSI_3 from *Synechocystis* and Red_a mutant 6803 *Synechocystis* strain,[25] in frame A the photoproduct is shifted to *lower energies* (see the asterisk in frame A). The inset

https://doi.org/10.1021/acs.jpcb.2c04829
J. Phys. Chem. B 2022, 126, 6891–6910

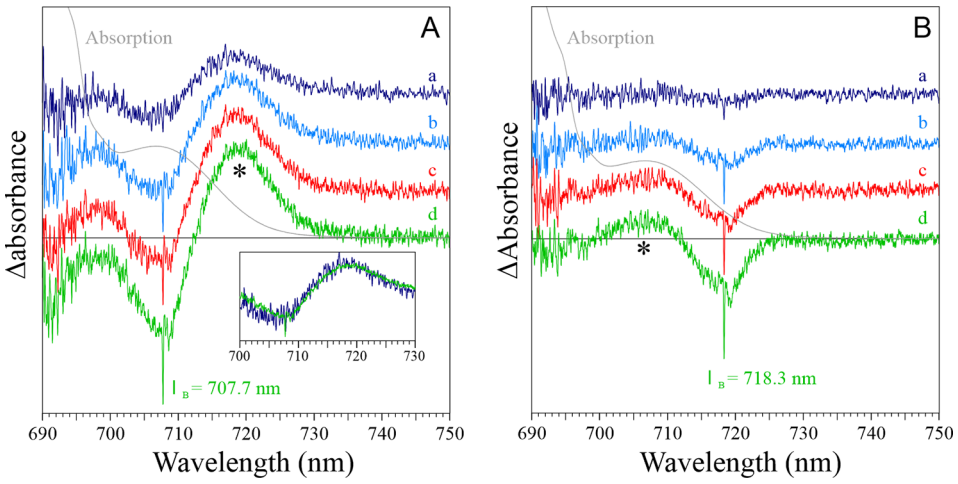

Figure 7. Persistent holes in the red state region. (A) Curves a-d were obtained for the PSI_3−$IsiA_{18}$ supercomplex with λ_B of 707.7 nm. The inset compares normalized (and scaled) curves a and d at the maximum of the antihole. (B) HB spectra obtained for λ_B = 718.3 nm. The 5 K spectra a−d in both frames A and B were obtained with an increasing burning fluence of 3.6, 10.8, 25.2, and 54.0 J/cm^2, respectively. The asterisks indicate photoproduct location.

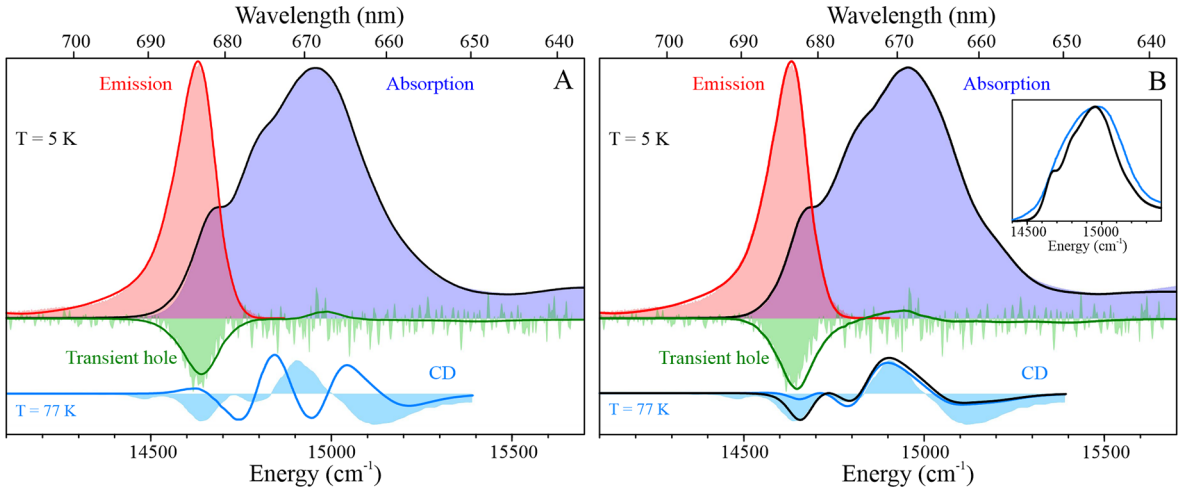

Figure 8. (A) Filled curves are experimental absorption, emission, and transient (nonresonant) HB spectra of IsiA monomers at T = 5 K. Emission/HB spectrum were obtained for λ_{ex} /λ_B of 665.0 nm. Solid lines are the best fits to our spectra, obtained for model *MA* assuming the absence of Chls 517/501 and 70% loss of Chl 511. Filled lower curve and a superimposed solid blue line correspond to the experimental[15] and calculated (this work) CD spectra at 77 K. (B) Filled curves are the same experimental spectra of IsiA monomers as in the left frame. Solid lines are model curves using model *MB*. In this case, the best fits are obtained assuming the absence of Chls 508/517 and 70% loss of Chl 511. The calculated CD spectra, represented by the solid blue and black lines, assume 70% loss and 100% occupation of Chl 511. Inset compares our 5 K absorption spectrum (black) with the 5 K spectrum reported in ref 15 (blue line).

compares curves a and d normalized at the maximum of the antihole. This comparison suggests that at the burn wavelength of 707.7 nm there are likely two independent bleaches of Chls with weak and very strong electron−phonon coupling, respectively, with the latter one showing higher HB yield. Frame B in Figure 7 shows HB spectra obtained at λ_B = 718.3 nm. Spectra a-d in both frames were obtained with an increasing burning fluence at T = 5 K (i.e., 3.6, 10.8, 25.2, and 54.0 J/cm^2); see also Section 5.2.

4. THEORETICAL MODELING OF OPTICAL SPECTRA

4.1. Modeling of Isolated IsiA Monomers. Filled curves in both frames of Figure 8 show experimental absorption (purple), emission (pink), and transient HB (green) spectra of the extracted population of individual IsiA monomers. In modeling of these spectra, we assume that (i) isolated monomers contain equal amounts of IsiA complexes from all possible locations within the $IsiA_{18}$ ring and (ii) isolated monomers maintain their native coupling coefficients (between pigments present) as their protein scaffolding should remain unchanged, although some more externally bound Chls could be lost. As mentioned above, all V_{nm} parameters for individual monomers h, n, o, p, q, and r are calculated using Tr-Esp methodology;[40] see Tables S3−S8 in the Supporting Information. For averaged V_{nm} values for h−r monomers, see Table S9 in the Supporting Information. Since the spectra for each type of monomers (i.e., h, n, etc.) are not available, the experimental spectra of isolated IsiA monomers are fitted with all 18 sets of V_{nm} values obtained for individual monomers of the ring. (The obtained Chl site-energy parameters are subsequently used in the hexamer calculations, vide infra.) The standard deviations in V_{nm} values of equivalent monomers

https://doi.org/10.1021/acs.jpcb.2c04829
J. Phys. Chem. B 2022, 126, 6891−6910

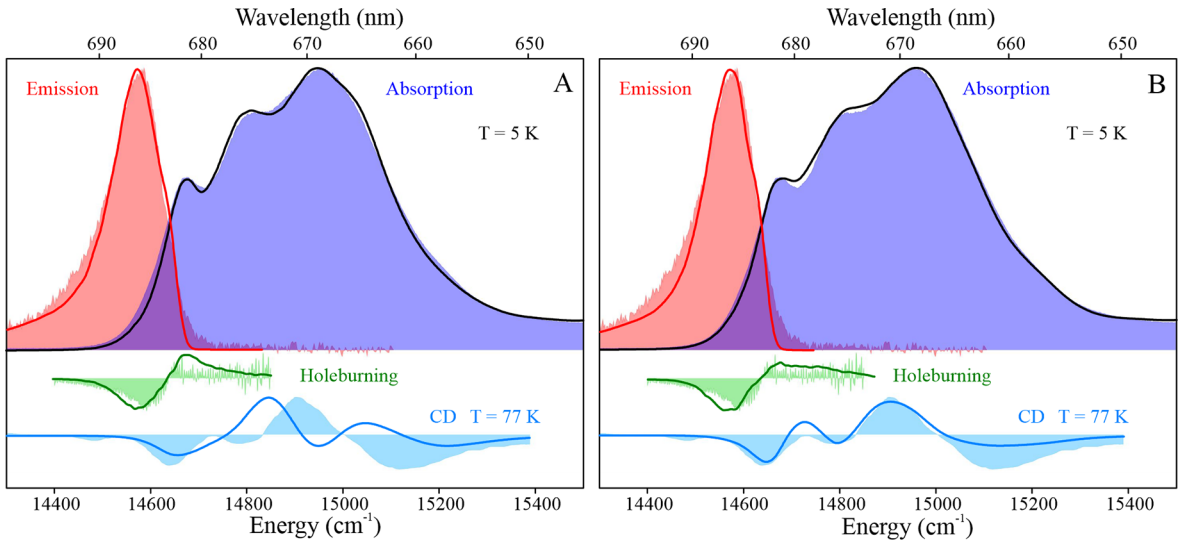

Figure 9. Top three filled curves are 5 K experimental absorption (purple), emission (pink), and nonresonant hole-burning of the $IsiA_{18}$ ring. Light blue curves are the 77 K CD spectra obtained for IsiA monomers.[15] Solid lines represent respective numerical calculation for $IsiA_{6(h\text{-}r)}$ hexamer (i.e., for monomers: h, n, o, p, q, and r) with 102 Chls total. Fits (solid lines) were obtained for models *HexA* (A) and *HexB* (B). The shapes of scaled experimental and calculated CD spectra are more similar in model *HexB*.

(due to C3 symmetry of the ring, i.e., W, n, and t in different hexamers) are smaller than variances in the V_{nm} values obtained for monomers in a hexamer (i.e., in $IsiA_{6(h\text{-}r)}$; see Table S10 in the Supporting Information). In other words, V_{nm} values of monomers in equivalent positions within the ring are more similar than those obtained for different monomers in a particular hexamer. In fact, we found only five large V_{nm} (V_{nm} > 10 cm^{-1}) in equivalently located monomers (W, n, and t), for which the standard deviation exceeded 15% of the V_{nm} value.

The solid lines in Figure 8 are the best fits to the experimental data. (All external Chls were considered as likely missing pigments in isolated IsiA monomers). In the left frame, all solid lines are obtained using coupling constants calculated for monomer "n". The best fits of absorption, emission, and HB spectra were obtained assuming that IsiA monomers do not possess Chls 501 and 517, while Chl 511 is present only in 30% of IsiA monomers (model *MA*). Very similar fits were obtained for other monomers, calculated with corresponding coupling constants (data not shown). Filled lower curve and a superimposed solid blue line correspond to the experimental[15] and calculated 77 K CD spectrum. Note that CD spectrum was obtained in ref 15 for different sample and was not fitted as part of the overall fitting procedure reported here. However, the set of parameters obtained in model *MA* cannot provide a good qualitative match to the CD spectrum. The right frame shows another fit of the same experimental data (model *MB*), which can describe the CD spectrum. Here the best fits are obtained assuming absence of Chls 508 and 517 and 70% loss of Chl 511. The calculated CD spectrum represented by the solid blue line assumes that Chl 511 is present in 30% of IsiA, while the black CD curve assumes 100% presence of Chl 511. Thus, it appears that sample studied in ref 15 had a full occupation of Chl 511. None of the other combination of missing Chls could simultaneously describe our experimental data. Thus, we conclude that model *MB* is consistent with the experimental data. Note that model *MB* is feasible as the missing Chls 508/517 are located between ring's monomers (see Figure 2) and could be lost in isolated IsiA complexes. All fits in Figure 8 were obtained with the phonon Huang–Rhys factor, S = 0.55 (estimated from HB data) and sum vibrational Huang–Rhys factors S = 0.29 for absorption and S = 0.3 for emission. Exciton energies and their standard deviations averaged over all 18 monomers are shown in Table S11 in the Supporting Information.

Both experimental and calculated (scaled) CD curves in Figure 8 were obtained for IsiA monomers. Since the number of Chls likely differed (vide supra) as reflected by somewhat different absorption shapes (see inset in Figure 8B) and our calculated CD curve is based on parameters from fits of 5 K data, whereas the experimental CD was measured at 77 K, no perfect agreement was anticipated. However, the calculated shape is in better qualitative agreement in model *MB*.

4.2. Modeling of the $IsiA_6$ Hexamers. Below we model the absorption (curve c′, Figure 3B) and emission spectrum with a maximum at 686 nm (black curve, Figure 3C), assigned above to the $IsiA_{18}$ ring. We concentrate on the exciton structure and the energy landscape of Chls bound in the ring. Recall that the emission with a maximum at 724 nm corresponds to the PSI_3 trimer residing within the PSI_3–$IsiA_{18}$ supercomplex. For simplicity, we focus on structure-spectrum relationship of the six IsiA monomers labeled as h, n, o, p, q, and r, combined into hexamer ($IsiA_{6(h\text{-}r)}$; 102 Chls total), which encompass one PSI monomer of the PSI_3 trimer (see Figure 1). Based on the structural data[12] and the experimental data shown in Figure 3, we assume that each IsiA (intact) monomer within an intact $IsiA_{18}$ ring contains all 17 Chls.

The top three filled curves in Figure 9 (in both frames) are 5 K experimental absorption (purple), emission (pink), and nonresonant hole-burning of the $IsiA_{18}$. The solid cyan spectra in both frames are the same 77 K CD spectrum adopted from ref 15 and are shown here only for a comparison. The CD spectra were not part of the overall fitting procedure. Solid lines in the left and right frames represent the best fits to the spectra described above, using the hexamer $IsiA_{6(h\text{-}r)}$. To obtain the best fits, all earlier found E_o and fwhm values of 6 × 15 pigments (that were present in isolated monomers) were fixed and it was assumed that all pigments including Chls 501, 511,

https://doi.org/10.1021/acs.jpcb.2c04829
J. Phys. Chem. B 2022, 126, 6891–6910

and 517 (model *HexA*) or Chls 508, 511, and 517 (model *HexB*) are present at 100%. Thus, in this case, the only optimizable parameters were E_o and fwhm values for pigments 501/517 (or 508/517) as the parameters of Chl 511 remained the same. The best fits for model *HexA* are obtained using following E_o and fwhm values: for Chl 501, (14851 and 157 cm^{-1}), and for Chl 517, (14992 and 105 cm^{-1}). E_o/fwhm values in model *HexB* were for Chls 508 and 517 are 14991/106 $cm^{-1}$and 14769/185 cm^{-1}, respectively.

Again, Model *HexB* (Figure 9B) appears to be more consistent with the experimental data (see Section 5.4 for discussion). We emphasize that the CD spectra were calculated after simultaneously fitting absorption, emission, and HB spectra, clearly indicating that that the agreement for the *MB* and *HexB* models is not forced by the algorithm. Very similar energy landscapes and fits of spectra shown in Figure 9 were obtained for two other sets of the ring's hexamers consisting of monomers ($IsiA_{6(W, X, Y, Z, g, y)}$ and $IsiA_{6(t, u, s, w, r, v)}$). Averaged exciton energies (horizontal lines) for models *MB* (left) and *HexB* (right) are shown in Figure S3 in the Supporting Information. Quite large interpigment distances render respective couplings weak enough, so that a few percent of change in coupling strengths does not change spectral shapes of studied complexes much.

4.3. Modeling of the $IsiA_{18}$ Ring. Calculated spectra (solid lines) for the entire $IsiA_{18}$ ring (18 monomers) are shown in Figure 10. The top three filled curves are 5 K

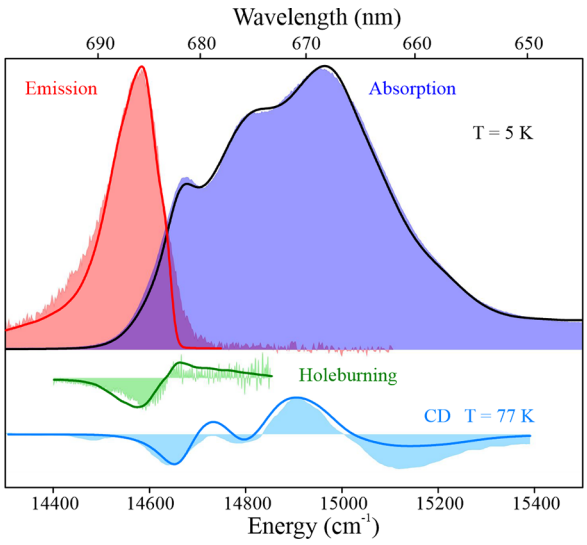

Figure 10. Top three filled curves are 5 K experimental absorption (purple), emission (pink), and nonresonant hole-burning of the $IsiA_{18}$ ring (this work). Light blue filled curve is the 77 K IsiA CD spectra from ref 15. Solid lines represent respective numerical calculation for the entire $IsiA_{18}$ ring.

experimental absorption (purple), emission (pink), and nonresonant hole-burning of the $IsiA_{18}$ ring (adopted from Figure 9). The light blue filled curve is the 77 K CD spectra from ref 15. (We emphasize that the CD spectra will not be involved in the overall fitting procedures discussed below.) Exciton energies and their standard deviations averaged over all monomers within the ring are shown in Table S10 in the Supporting Information. Exciton states of isolated IsiA monomers and intact monomers within the supercomplex ring are also discussed in the Supporting Information. Calculations were made for 306 pigments (200k iterations), using *HexB* model for all three hexamers.

All hexamer site-energies, inhomogeneities, S-factors, and spectral densities were included into the model without any change from the respective three *HexB* Hamiltonians. Absorption spectrum and CD spectrum amplitudes are in the same scale, normalized to unity for absorption. Only emission calculation differed from the hexamer model, because the emission spectrum does not scale up if one adds monomers, and this is why. In a purely excitonic approach, emission occurs only from the very lowest-energy exciton state, as it is assumed that relaxation is several orders of magnitude faster than the emission lifetime. Consequently, such (purely excitonic) emission spectrum in full $IsiA_{18}$ ring would be red-shifted and much narrower than experimentally observed emission. For $IsiA_{18}$ ring, the assumption of full excitonic relaxation to the very lowest state is clearly invalid, as EET may or may not be possible between the lowest states of the 18 IsiA monomers. As argued above, EET between monomers is much slower than intramonomer exciton relaxation; i.e., it occurs via Förster mechanism and most likely has not more than 2−4 intermonomer crossings. Thus, in terms of Redfield/excitonic approach, one needs to allow some emission from the lowest exciton states of various IsiA monomers. The best fit of the experimental curve was obtained assuming that 27% emission originates from the lowest exciton state, 37% emission is monomeric in nature (i.e., it comes from the lowest state in particular monomer, without any EET) and 36% of light comes from exciton states 2−7 (i.e., after a few steps of intermonomer EET, but not fully relaxed).

4.4. Averaged Site Energies and Averaged Inhomogeneities (Γ_{inh}). The local protein environment surrounding various Chls produces disorder in site energies. At 5 K, slow thermal motion of the protein is largely frozen, leading to an inhomogeneous or static disorder (Γ_{inh}). Figure 11 shows simulated (averaged) site energies and Γ_{inh} obtained for Model *MB* for all IsiA subunits within the ring. Note that all site energies and Γ_{inh} that were free parameters in model *MB* and were fixed in model *HexB*. Both site-energies and SDF widths slightly differ from subunit to subunit, as indicated with red vertical bars in Figure 11, showing the standard deviation averaged over all subunits values. One can clearly see in Figure 1 that the ring possesses C3 symmetry. The C3 nature of the ring creates periodic differences in pigment positions and orientations, which carries over into (periodic) differences in coupling energies within and between subunits. Small differences between monomers are also reflected in estimated site-energy values for ring subunits. Site-energy values changing with period 6 can be observed for about half of the Chls (in both models *MA* and *MB*); as an example, the inset of Figure 11 shows fluctuation of site-energy values for Chl 502 and Chl 504. Periodic behavior is much less expressed for Γ_{inh}. (See Figure S4 and Table S10 in the Supporting Information for similar data obtained for models *MA* and *HexA*).

4.5. EET around the $IsiA_{18}$ Ring and from the Ring to the PSI_3 Core. Based on the above discussion, model *HexB* appears to offer a better fit between the simulations and experimental results, especially the CD spectra. Therefore, our analysis of the energy migration around the $IsiA_{18}$ ring and from the ring to the PSI_3 core mostly focused on model *HexB*. (Some results for model *HexA* will be shown for comparison.) Calculations were performed using a simplified model where intramonomer relaxation is assumed to be fast enough (see

https://doi.org/10.1021/acs.jpcb.2c04829
J. Phys. Chem. B 2022, 126, 6891−6910

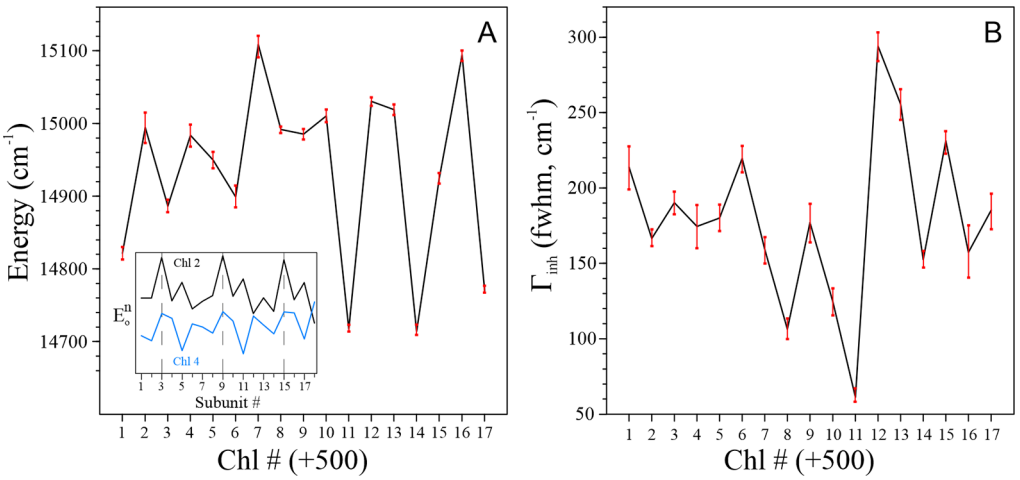

Figure 11. Frame A: Site energies of 17 Chls resulting from the fit of the monomer spectra and averaged over all 18 subunits of the supercomplex ring; Frame B shows similarly obtained and averaged Γ_{inh}. Red error bars indicate calculated standard deviation. For a number of pigments, there is a systematic change with period 6 in site-energy values indicating C3 symmetry of the ring. The inset in the left frame shows such periodic behavior for Chl2 and 4 site-energies, E_n^0. Numbers 1−17 on the *x*-axis correspond to Chls 501−517, i.e. Chl # (+500).

Table S14) and only four lowest-energy pigments per IsiA monomer contribute to the IsiA$_{18}$ ring emission or transfer energy to the adjacent IsiA monomers or to the PSI core. In model *HexB*, these pigments are 514 (42.8%), 511 (26.4% with a narrow SDF of 61.2 cm^{-1}), and 517 (10.8%), followed by 501 (7.5%); for details, see Table S14. We find that in model *HexB* pigments 511 (previously referred to as Chl 44)[30] and 514 (a.k.a. Chl 37) are switched compared to our earlier assignment for CP43 complex with smaller number of Chls.[30] The inhomogeneous broadening of Chls 511 and 514 is so different that in most cases Chl 514 (equivalent to Chl 37 in CP43) is the largest contributor to the lowest state. As (intramonomer) couplings between the above four pigments are relatively weak, in the first approximation we assume that the lowest-energy state in model *HexB* is weakly delocalized. That is, we assume that excitation is localized on one pigment or another, but which particular pigment it is varies from monomer to monomer due to different realizations of the static energy disorder. (This is less true for model *HexA* where the lowest state may be delocalized over Chls 501 and 502; data not shown for brevity.)

In modeling the intermonomer EET processes, we started from SDF parameters obtained from the fits of various types of optical spectra as discussed above. These SDF parameters were determined using the algorithm involving so-called vertical energies. Therefore, the above SDF were red-shifted by 29 cm^{-1} to arrive at the ZPL-based SDF, as required by the model developed in ref 35. The shift is based on the electron−phonon coupling parameters. Next, the distributions of the oscillator strength of the four Chls with the strongest contribution to the lowest-energy state were calculated using the Monte Carlo approach (see Figure 12A). The sum of all 17 such distributions is equal to the sum of all 17 excitonic states and can serve as the SDF for the absorption spectrum. Four distributions in Figure 12A were used as the SDFs for the subsequent calculations, including for calculating the probabilities of finding the pigments of each type at frequency lower than the given frequency. It was also verified that the SDF of the lowest state of the 4-pigment simplified system was a nearly perfect match to the lowest-energy state of the 17-pigment model. (Three pigments were not enough from that perspective.) Note that all curves in Figure 12A except for Chl 501 feature a single maximum with the integral intensity close to that of an isolated Chl, further indicating that respective states are weakly delocalized.

Figure 12B shows contributions of Chls 511, 514, 517, and 501 to the lowest-energy state of the intact (17-pigment) IsiA monomer. The red curve in the inset in Figure 12B represents the wavelength-dependent probability that there will be at least one lower-energy pigment in the neighboring two IsiA monomers (eight possibilities total). At the peak of the intact monomer's lowest state SDF (black curve in the inset; can be localized on either 501, 511, 514, or 517; see Table S14), the probability to have at least one further acceptor within the IsiA ring is still as high as 0.8. Of course, the lower the energy of the donor, the smaller is the probability to find any suitable acceptors. Note that the red curve is obtained under the assumption that all eight intermonomer EET times are short and the only condition for EET is the availability of the lower-energy acceptor(s).

Perfect EET from the IsiA$_{18}$ ring to the PSI core would result in no emission at 686 nm, in clear disagreement with the experiment. Structural data also indicate that Chls of some IsiA monomers are far from the core Chls (Figure 2). Let us therefore consider an intact IsiA monomer that is part of the IsiA$_{18}$ ring (and therefore is not missing any pigments) but does not directly transfer energy to the PSI core. Let us call it a type-1 monomer. The emission-origin ZPL-based SDFs of the lower-energy Chls in the type-1 monomer are shown in Figure 12C. Each of them was obtained via multiplying the respective SDF in Figure 12B by the sigmoidal curves representing the probabilities of only the relevant (fast-enough, see below) acceptors *in both neighboring IsiA monomers* to be lower in energy. These sigmoidal curves were based on the respective full SDFs shown in Figure 12A. The type-1 monomer emission will be significantly red-shifted with respect to that of the intact *isolated* monomer (without missing Chls), by about 21 cm^{-1} or 1 nm (comparing the black curve in the inset of Figure 12B and the brown curve in Figure 12C). One can estimate the fractions of energy emitted from type-1 monomer (about 45%) and transferred to the neighboring monomer(s) (about 55%)

https://doi.org/10.1021/acs.jpcb.2c04829
J. Phys. Chem. B 2022, 126, 6891−6910

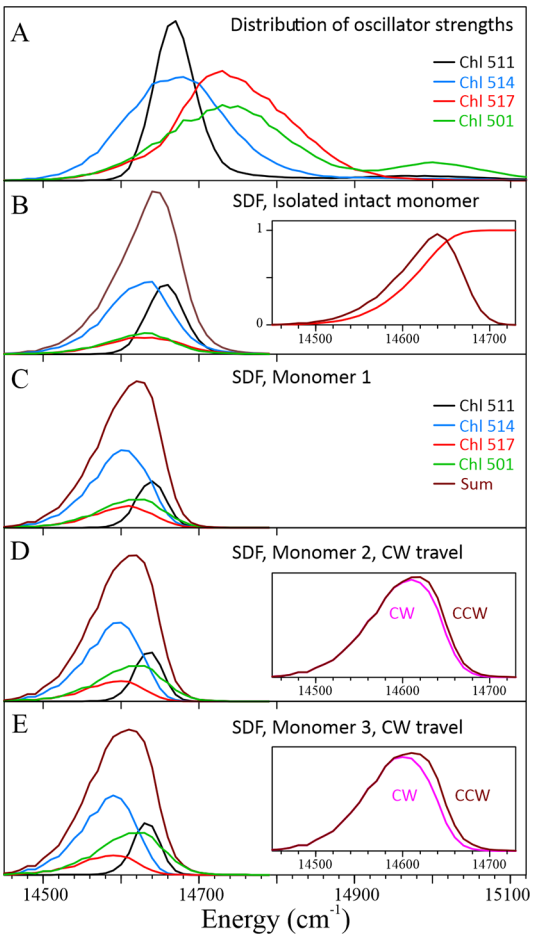

Figure 12. Model *HexB*. (A) Distributions of oscillator strength belonging to Chls 511 (black), 514 (blue), 517 (red), and 501 (green). Depicted curves represent SDF defined as the probability to find the ZPL at given frequency (not "vertical energies"). Multipeaked curves reflect excitonic interactions, e.g., a strong coupling between Chls 501 and 502. (B) Contributions of the above pigments to the lowest state of the intact IsiA monomer (no further EET). The insert depicts the lowest-energy state of such monomer (brown, the sum of black, blue, red, and green curves from the mainframe B) peaked at 14641 cm^{-1} and the wavelength-dependent probability of having at least one lower-energy pigment in one of the adjacent monomers (red). (C) Contributions of the above pigments to the SDF that is the origin of the emission of the type-1 IsiA monomer, incapable of a direct EET to the PSI core but capable of EET to adjacent IsiA monomers (see text for more details). Key: black, Chl 511; blue, Chl 514; red, Chl 517; green, Chl 501; brown, sum, peaked at 14620 cm^{-1}. (D) Same as in frame C but for the type-2 monomer, energy traveling counterclockwise "left" in terms of Figures 1 and 13. The insert depicts the difference between the brown curve (same as in the mainframe D) and similar curve for type-2 monomer, but for traveling "right" (clockwise, CW, magenta) in terms of Figure 1. (E) Same for type-3 monomer, traveling "left" (counterclockwise, CCW) in terms of Figure 1. The insert depicts the difference between the brown curve (same as in the mainframe E) and the similar curve for type-3 monomer, but for traveling "right" (i.e., CW) in terms of Figure 1, magenta.

from the ratio of the integrals of the brown curves in Figure 12, parts C and B.

Average intermonomer EET times were determined using the Förster approximation as described in ref 47; the results are summarized in Figure 13. Two parts of this figure depict average EET times for two pairs of monomers, n−o and h−n (see Figures 1 and 2). In what followed, we use these EET times to determine how many potential energy acceptors in the adjacent IsiA monomers are actually available for each pigment. We utilized 1.1 ns average EET time (n−o 511−511 EET time) as a cutoff; i.e., slower EET processes were ignored in these calculations. Although the radiative lifetimes for the four Chls involved are not known, they are most likely longer than 1.1 ns. Note that although some EET times differed by as much as a factor of 20, for example o514 → n517 and n514 → h517; all the fast-enough EET channels were the same for both IsiA monomer pairs. Next, we adopted the approach described previously in ref 54 to model the shapes of the sub-SDF of the four relevant pigments that are contributing to the ring emission in different scenarios involving EET around the $IsiA_{18}$ ring and to the PSI_3 core.

Figure 14A depicts a scenario where three evenly spaced entry points for $IsiA_{18}$−PSI_3 EET are present per PSI core monomer. The monomer that is capable of transferring energy to the PSI core is labeled as the type-0 monomer. (Numbers in the rings in Figure 14 indicate monomer types.) Note that due to the C3 symmetry of the supercomplex, all percentages here and below are the same for (a) the $IsiA_6$ hexamer and PSI core monomer and (b) the supercomplex containing the $IsiA_{18}$ ring and the trimeric PSI_3 core. In this case, all emission of the $IsiA_{18}$ ring will be from type-1 monomers, and emission will account for about 11% of the total supercomplex emission (ignoring possible differences in fluorescence yields of various core and IsiA pigments/states). However, the relative intensity of the $IsiA_{18}$ emission observed in our experiments on $IsiA_{18}$−PSI_3 supercomplexes (see Figure 3) is higher than 11%.

Next, we assumed that energy, while potentially capable of moving from our type-1 monomer in either direction, moved to the next monomer on the left. (Clockwise, CW, energy travel is briefly addressed below.) If that IsiA monomer also cannot transfer energy to the PSI core (we call this kind of monomer type-2 monomer; in general, the "type-*N* monomer" is an IsiA monomer incapable of EET to the PSI core that is reached from type-1 monomer in $N - 1$ steps), then the probability of finding suitable further acceptors in the IsiA ring will be much lower, for two reasons: first, we are now, on average, at lower energy than we were in the type-1 monomer; second, excitations can only move further in one direction. Excitation cannot return to the type-1 monomer, as in this model all its pigments are higher in energy. The emission of the type-2 monomer will be somewhat red-shifted with respect to the emission of the type-1 monomer, and the probability of the emission will be much higher (i.e., about 78 or 82%, depending if excitation moves clockwise (CW) in terms of Figures 1 and 13 or counterclockwise (CCW) along the ring, respectively). The brown curve in Figure 12D represents the ZPL-based SDF serving as the emission origin for type-2 (moving CCW). The magenta curve in the inset of Figure 12D represents the ZPL-based SDF for the type-2 monomer (moving CW). Assuming that the type-2 monomer is also incapable of the EET to the PSI core, we introduce the type-3 monomer. Brown curve in Figure 12E represents the ZPL-based SDF serving as the emission origin for type-3 monomer (moving CCW). Magenta curve in the inset of Figure 12E represents the ZPL-based SDF for type-3 monomer (moving CW). Emission probabilities at this step are 82 or 87%, for moving CW or CCW, respectively. Note that the brown and magenta curves are different, which reflects different numbers of acceptors that are actually available (taking into account the

https://doi.org/10.1021/acs.jpcb.2c04829
J. Phys. Chem. B 2022, 126, 6891−6910

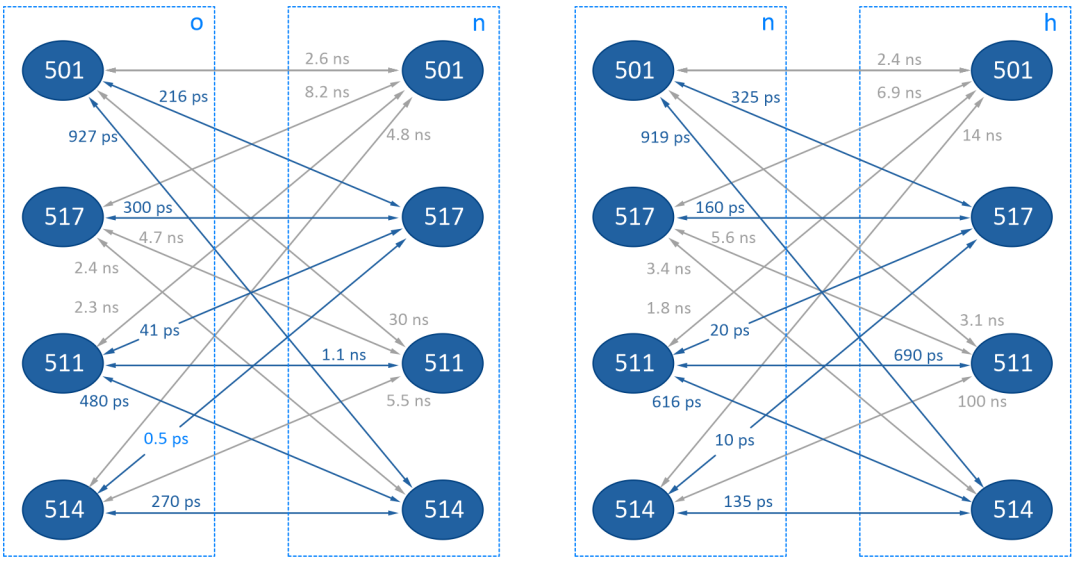

Figure 13. Average Förster intermonomer EET times for model *HexB* for monomer pairs n−o (left) and h−n (right). EET times are subject to distribution due to the distribution of spectral overlaps.[46,47] For the same pair of pigments, differences in average EET times for "left" and "right" travel are up to 10% and arise from differences in the distribution of spectral overlaps that in turn result from the differences in the SDF parameters of the four lowest-energy pigments. All arrows are bidirectional because depending on the realizations of disorder any Chl could be at lower energy (see text for details).

EET times) when traveling along the ring in the opposite directions. Type-3 monomer SDF is slightly narrower and more red-shifted in the case of traveling "right" (CW), leading to better eventual agreement with the experiment. The respective type-3 monomer emission (not shown) would be peaked at 686.3 nm for CW travel as opposed to 685.8 nm for CCW travel. We can now consider a scenario where there is only one EET entry point between $IsiA_6$ hexamer and PSI core monomer. We illustrate this scenario in Figure 14B. Here, the $IsiA_{18}$ ring almost does not transfer energy to the PSI_3 core (i.e., only 23% of the energy absorbed by the ring is transferred) and the $IsiA_{18}$ ring emission should account for over 38% of the total supercomplex emission, clearly a much larger percentage than observed in our experiments. The final emission-origin SDF will be the weighted sum of one type-1 monomer SDF, two type-2 monomer SDFs (for moving CCW and CW) and two type-3 monomer SDFs (for moving CCW and CW in terms of Figure 1). The respective weights are given by the red numbers in Figure 14.

Two scenarios involving two well-separated entry points per PSI core monomer (with one or two IsiA monomers separating these entry points (Figure 14 , parts C and D) result in 24.5% of the supercomplex emission originating from the $IsiA_{18}$ ring. Note that in order to obtain narrower and more red-shifted emission spectra, one needs to include a significant contribution from type-3 monomer emission, particularly for CW travel (see inset of Figure 12E), making scenario D slightly more likely than scenario C (which does not involve emission from type-3 monomers). Figure 14E depicts a scenario with two adjacent IsiA monomers serving as the only entry points. Here, IsiA ring emission is expected to contribute over 29% to the whole supercomplex emission. Finally, in a scenario depicted in Figure 14F, an additional well-separated entry point is added to the scenario in Figure 14E, resulting in IsiA contributing 16% to the supercomplex emission, in good agreement with our experimental data shown in Figure 3. Summarizing, emission probabilities for model *HexB* are 45% for type-1 monomer, 78/82% for type-2 monomer traveling CW/CCW, and 82/87% for type-3 monomer traveling CW/CCW. See Figure S5 in the Supporting Information, which shows the SDF serving as the emission origin for the scenario depicted in Figure 14D for model *HexB* and preferentially CW (darker colors) and CCW (lighter colors) travel.

5. DISCUSSION

5.1. Low-Temperature Absorption and Emission Spectra. Regarding somewhat larger oscillator strength of the low energy trap(s) of PSI_3 core residing within the $IsiA_{18}$ ring of the supercomplex, we hasten to add that small protein structural differences between PSI_3 trimer grown under normal and iron-deficient conditions, leading to a weaker oscillator strength of the low-energy trap(s) and blue-shifted and broader PSI_3 emission, cannot be entirely excluded (compare the maxima in spectra a_{flu} and b_{flu} at 721.7 and 724.0 nm, respectively, in frame C of Figure 3). We suggest, based on preliminary calculations (to be discussed elsewhere) that the emission shift toward the red observed for intact PSI_3 residing within the supercomplex is likely caused by interactions between the $IsiA_{18}$ ring and the three monomers of PSI_3 trimer. However, it is unlikely that PSI core complex is deformed by the surrounding ring. A more likely scenario is that the red-most states of the PSI core have a strong CT character. Such states are sensitive to local environment and changes in growth conditions could cause noticeable differences in optical spectra. This is consistent with the broadening and red-shifting of the fluorescence (with a maximum near 724 nm) and absence of ZPH in the low-fluence resonant hole burned in the supercomplex with λ_B = 707.7 nm (see Figure 7). Of course, we cannot entirely exclude that there is a small oscillator strength redistribution among low-energy Chls of the PSI_3.

5.2. Hole-Burned Spectra. To calculate the nonresonant HB spectrum, we assumed that each pigment's pre- and postburn site-energy distributions are exactly the same—only

https://doi.org/10.1021/acs.jpcb.2c04829
J. Phys. Chem. B 2022, 126, 6891−6910

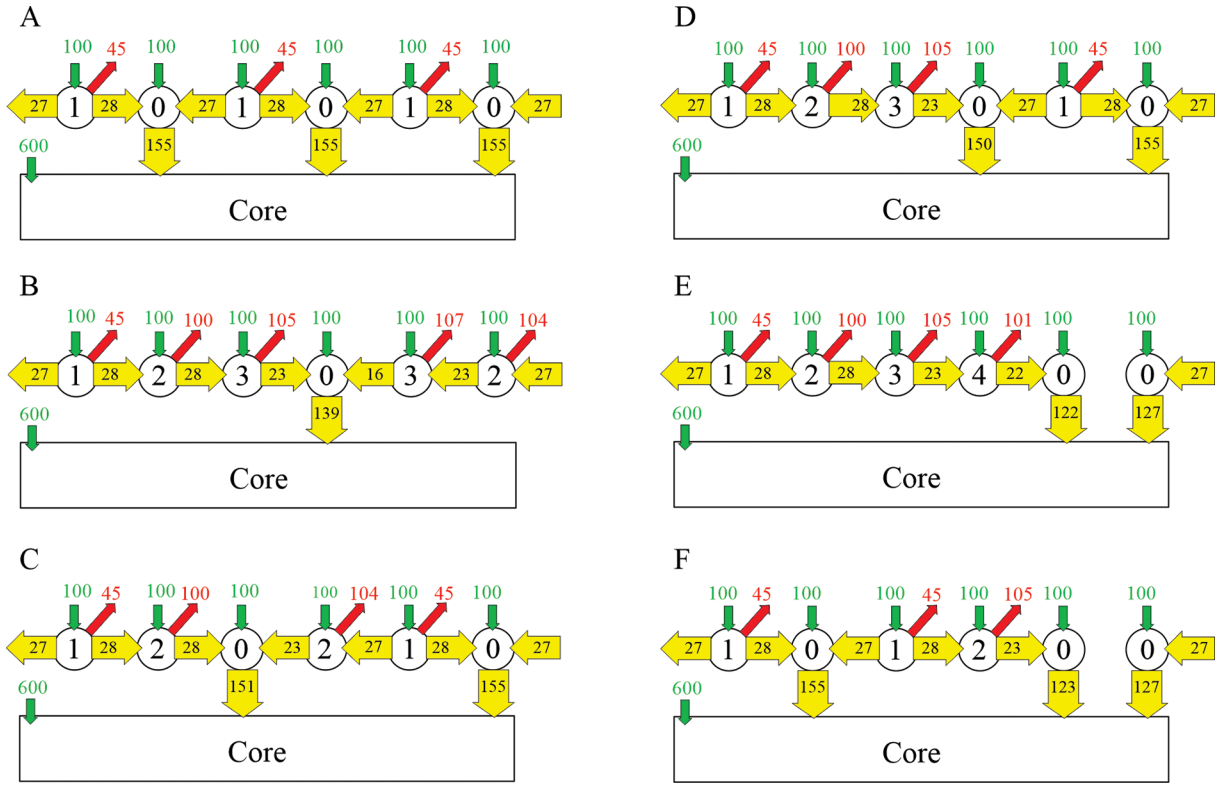

Figure 14. Possible scenarios for EET between the IsiA monomers within the $IsiA_{18}$ ring and from the $IsiA_{18}$ ring to the PSI_3 core. Only six IsiA monomers (numbered according to the "type", see text for details) and one PSI core monomer are shown for brevity. It is assumed that each IsiA monomer absorbs 100 photons while one PSI core monomer absorbs 600 photons (green numbers and arrows). Numbers in yellow arrows indicate EET between adjacent monomers (or EET into PSI core). Red numbers indicate number of photons emitted from the respective IsiA monomer due to finite efficiency of EET. Depicted numeric values are calculated for model *HexB*. In case A, there are three evenly spaced entry points per PSI core monomer and $IsiA_{18}$ ring emission is expected to contribute about 11% to the total emission of the PSI_3–$IsiA_{18}$ supercomplex. In case B, there is only one entry point per PSI core monomer, and the $IsiA_{18}$ ring is expected to contribute about 38% to the total emission of the $IsiA_{18}$–PSI_3 supercomplex. Cases C and D depict two possible examples with two well-separated entry points per PSI monomer. In cases C and D, emission of the $IsiA_{18}$ ring comprises 24.5% of the supercomplex emission. In the case E, the IsiA hexamer has two adjacent entry and the ring emission should account for 29% of the total supercomplex emission. In the case F, the IsiA hexamer has two adjacent and one additional entry points, and the ring emission should account for 16% of the total supercomplex emission.

energy realizations for pre- and postburn differ. That is, the burning pigment (changing its energy upon tunneling) was selected according to its probability to contribute to the thermally occupied (at 5 K, mostly the lowest) exciton state. No parameters are further optimized to obtain the NRHB spectrum; i.e., we used the same Hamiltonian as that to fit the absorption and emission spectra, as well as to calculate the 77 K CD spectrum.

It is known that illumination of PSI samples may result in the formation of persistent (at cryogenic temperatures) $P700^+$ minus P700 spectrum.[52,53] This issue has been extensively explored for *Synechocystis* PCC6803 as well as *Thermosynechococcus elongatus*.[53] In that work, three types of (non iron-deficient) samples were explored—"reduced" (referring to full reduction of F_A and F_B clusters with dithionite), "oxidized" (referring to the state of P700, obtained by cooling sample down under white light illumination), and "partially reduced" (a smaller concentration of dithionite was used to avoid full reduction of the F_A and F_B clusters, and all possible effort was made to keep the samples in complete darkness prior to the measurement.) The "reduced" and "oxidized" samples exhibited negligible persistent $P700^+$ minus P700 signatures. The latter had P700 already oxidized, and in the former, the recombination from terminal acceptor F_X occurs within milliseconds.[52,55,56] Only the samples that were cooled in the dark exhibited significant $P700^+$ minus P700 signatures. These signatures could be produced by exceedingly weak illumination, such as exposure to the dimly lit room, several nW/cm^2 at all wavelengths combined. Such intensities do not cause any measurable NPHB. This is expected, since the yield of charge separation is close to one for excitation wavelengths shorter than 700 nm, while the NPHB yield is on the order of 10^{-4}–10^{-5} in chlorophyll–protein complexes.[47,57,56] Absorption and NPHB spectra in this work were measured with FTIR spectrometer. In such a spectrometer, intensity of white light (kept constantly on the sample) is at least tens of μW. Recall that our samples contained no dithionite. Thus, our complexes were "oxidized" in terms of refs 52 and 53, and no interference between $P700^+$ minus P700 and NPHB holes was detected (see Figure S7 in the Supporting Information). It was also previously reported that, unlike in *T. elongatus*, in *Synechocystis* PCC6803 P700 oxidation does not cause the shift of the emission, only reduction of its intensity.[53] Thus, small difference in the emission peak wavelengths between the trimeric PSI and the $IsiA_{18}$–PSI_3 supercomplex is unlikely due to incomplete oxidation of P700 in one of the samples.

Note that the T_1 values are related to the so-called homogeneously broadened line widths, Γ_{hom}, where Γ_{hom} =

https://doi.org/10.1021/acs.jpcb.2c04829
J. Phys. Chem. B 2022, 126, 6891–6910

$^1/_2\Gamma_{ZPH}$.[34,35] A good approximation is that $T_1 \sim (2\pi c\Gamma_{hom})^{-1}$, since pure dephasing T_2* is a minor contribution at T = 5 K in the presence of fast enough EET.[34,35] The higher resolution (i.e., 0.5 cm^{-1}) ZPH burned in the supercomplex at λ_{B2} = 686.0 nm with fwhm of the ZPH of 1.2 cm^{-1}, shown in Figure 5A, corresponds to a T_1 value (resolution corrected) of 11 ps. The 683.1 nm burning in a population of IsiA$_1$ monomers (spectrum c in Figure 5B) reveals mostly the ZPH and corresponding phonon sideband, as the lowest energy state and corresponding emission in the IsiA monomers are slightly blue-shifted from 683.2 to 683.5 nm. However, comparison of spectra b and c in Figure 5B shows that EET between the lowest energy states of IsiA monomers, as indicated by the broad shoulder building on the pseudophonon sides and near 685 nm, also takes place. Persistent resonant HB spectra obtained for λ_{B1} = 670.0 nm (blue) and λ_{B2} = 683.6 nm (red curve) using 1 cm^{-1} spectral resolution are shown in Figure 6B. The corresponding fwhm of the ZPHs burned at λ_{B1} and λ_{B2} in isolated monomers (see Figure 6B) correspond to the excited state lifetimes T_1 of about 4 and 11 ps, respectively. (Note, most of the intermonomer EET times are about tens or hundreds of picoseconds, which is an order of magnitude slower that intramonomer exciton relaxation, thus their possible contributions from the respective ZPHs are not resolved). Frame B in Figure 7 shows HB spectra obtained at λ_B = 718.3 nm. Spectra a−d in both frames were obtained with an increasing burning fluence at T = 5 K. The HB spectra (a−d) in Figure 7B are most likely burned into the lowest energy C714 trap of PSI$_3$ trimer, as they are similar to those observed (for similar burning wavelength) in isolated WT PSI$_3$ trimer.[25] This suggests that the configurational energy landscape of the Chls constituting the C714 trap *per se* is unaffected by the addition of the IsiA$_{18}$ ring. However, comparison of the HB spectra shown in Figure 7, parts A and B, reveals that the energy landscape of Chls absorbing at 707.7 and 718.3 nm varies significantly.

5.3. Isolated IsiA Monomer. The inset in Figure 8B compares our absorption spectrum (black curve) with that reported in ref 15, the blue curve. Note that 5 K absorption spectrum reported in ref 15 is broader (blue line) and their 77 K CD spectrum has responses near 14490 and 15130 cm^{-1}. This suggests that their sample could be partly contaminated and/or contained more IsiA Chls. However, none of the models tested provided better simultaneous fits than those shown in the right frame of Figure 8. Interestingly, Chl 511 (a.k.a. Chl 44),[30] in Model *MB*, is characterized by a narrow inhomogeneous broadening of 66−71 cm^{-1} (see Table S10). Moreover, in both models, the best fits are obtained assuming that the above Chl is largely (70%) lost. We have suggested before that either Chl 511 (a.k.a. Chl 44) or 514 (a.k.a. Chl 37) might be also responsible for the narrow absorption band near 684 nm in CP43 complex extracted from spinach.[16,51] The intensity of the latter band also varied from sample to sample, suggesting that Chl 44 (a.k.a. 511) can be easily lost in IsiA monomers. Both models *MA* and *MB* are in very good agreement with experimental difference spectrum (c′−d) shown in Figure 4, implying that about 2.7 Chls are absent in the individual IsiA complexes. The latter is consistent with the observed blue-shifted monomer emission in comparison with the red-shifted IsiA$_{18}$ ring emission (686 nm) and sample dependent maxima of single monomer fluorescence spectra (varying from 682 to 685 nm), as reported in the literature.[15,30] Although both models describe well the absorption, emission, and transient HB spectra, model *MB* yields much better agreement between calculated and experimental CD spectra.

5.4. IsiA$_6$ Hexamers and IsiA$_{18}$ Ring. Absorptive spectra (e.g., absorption and hole-burning) are additive spectra, and thus as soon as all six unique IsiA monomers are included in the sum spectrum of any hexamer (no matter how the ring is split), the resulting spectrum should be similar to the spectrum of the full intact ring. Emission spectra, however, are sensitive to the coupling between monomers. In order to calculate the emission spectrum for the full ring IsiA$_{18}$, one needs to note that in this case the lowest exciton state splits into 18 lowest-energy states localized in different IsiA monomers (see also Section 4.3). If there is no coupling between ring's monomers, one would expect all 18 lowest states to emit independently with equal probability, resulting in intact monomer-like emission. In case of very strong coupling and ideal downhill EET process, one would observe much narrower and more red-shifted emission than was actually observed experimentally. Although the intermonomer EET takes place, it stops much earlier because: (i) there are likely two or three efficient energy entry-point into PSI monomer per IsiA$_6$ hexamer, as discussed above, and (ii) due to disorder, neighboring monomer's lowest energy state may be at higher energy. Considering this, it is not necessary to consider EET over subunits larger than hexamers. As the number of IsiA monomers increases in a multimer, the calculated emission maximum shifts to the red, allowing one to estimate the effective multimer size. Experimentally observed emission maxima for isolated monomer is at 14630 cm^{-1} and for the full ring it is at 14585 cm^{-1}—such a shift in emission maximum is obtained if excitation travels in either 3 or 4 monomers before it is either emitted or transferred to the PSI core. Following that logic, hexamer was selected as a basic block to model both absorptive and emissive full ring spectra. EET between monomers is partially exciton relaxation as the strongest couplings between Chls 514 and 517 on neighboring monomers are about ∼30 cm^{-1}. However, in model *HexB*, Chls 514 and 517 contribute significantly (42% and 11%, respectively) to the lowest state of intact IsiA monomer. Calculated exciton state lifetimes for few lowest states are in the order of 1.8 ps in model *HexB*, which agrees with fastest observed relaxation time 1.7 ps in ref 17. The Förster energy transfer times between Chls of two adjacent IsiA monomers are about few tens of picoseconds and up to few nanoseconds. Recall that we observed resonant holes burned into the region of lowest exciton states of the IsiA (λ_{B2} = 683.6 nm), indicating that there are subsets of supercomplexes in which the lowest ring state lifetime is longer than 11 ps. The best fits of the emission shape were obtained when about 35% of the emission occurred from the lowest exciton state of the hexamer, 30% of emission occurred without any intermonomer energy transfer, and 35% occurred from second to sixth exciton state, which provides a small blue-shifted shoulder in the emission spectrum consistent with our emission spectra.

Previous modeling studies of various optical spectra of the CP43′ monomers (a.k.a. isolated IsiA) using the uncorrelated EET model,[54] suggested that CP43′ monomers (in analogy to the isolated CP43 complexes of PSII core) possess two quasi-degenerate low-energy states, A′ and B′. Our analysis suggested that Chls mostly contributing to the lowest-energy A′ and B′ states must be located on the side of the CP43′ complex facing the PSI core, a finding that contradicted the model of Zhang et al.,[31] but was in agreement with the model

https://doi.org/10.1021/acs.jpcb.2c04829
J. Phys. Chem. B 2022, 126, 6891−6910

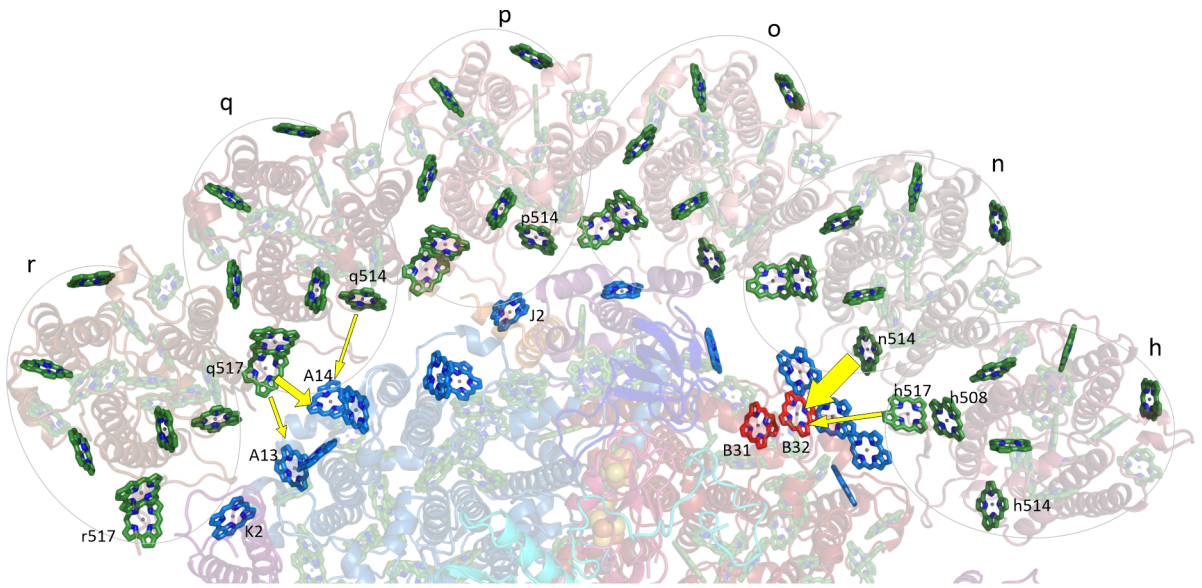

Figure 15. Possible major entry points from the hexamer to the PSI monomer in model *HexB*. The six IsiA monomers in Figure 14 (numbered according to the "type", see text for details) correspond to monomers r−h in Figures 2 and 15. Chls in blue and red correspond to PSI monomer; see text for details. Arrows indicate likely entry points for excitation from the ring to PSI monomer.

suggested by Nield et al.[33] Our arrangement is confirmed by recent Cryo-EM imaging studies.[12] Based on our previous excitonic calculations (based on the CP43 structure),[30] the best Chl candidates that contribute to the low-energy A′ and B′ states were Chl 44 and Chl 37, respectively. According to the nomenclature used in this work the latter Chls correspond to Chls 511 and 514, respectively (see Table S1 in the Supporting Information for the equivalence of different nomenclatures used in the literature). That is, we suggested in ref 51 that the lowest energy Chl 37 (514) in CP43 complex from spinach is the pigment characterized by a relatively narrow Γ_{inh} (73 cm^{-1}), while the second lowest-energy Chl 44 (i.e., 511) had larger Γ_{inh} by a factor of 2.57.[16] A similar assignment was reported for the CP43′ (IsiA complex) in ref 30; in this case, however, Γ_{inh} of state A′ was larger than that of state B′ by a factor of 2.25. At that time, however, CD spectra were not modeled. The best model in this work (i.e., *HexB* model) is consistent with the above data, though the lowest site energies (E_0) of Chls 514 (37) and 511 (44) are nearly identical. Namely, we found that the E_0/Γ_{inh} of Chl 514 (37) and Chl 511 (44) are 14713/153 cm^{-1} and 14717/61 cm^{-1}, respectively. Note that the assignment of the narrowest SDF is switched here compared to our earlier works. The third lowest energy pigment is the newly identified Chl 517 with E_0/Γ_{inh} of 14770/185 cm^{-1} (see Table S10 for details). That is, nearly identical site energies of Chls 514 and 511 and reversed extent of their inhomogeneities, provided the best fit of multiple spectra, including reasonable fit of CD spectra from ref 15. Current modeling reveals that Chl 511 (i.e., 44) has a smaller inhomogeneity (by a factor of 2.5) than Chl 514 (37). Note that the coupling constant between Chls 514−517 of neighboring monomers of about 30 cm^{-1} accommodates very efficient EET between monomers (vide infra) as their energies are similar and there is relatively large spectral overlap.

5.5. EET around the $IsiA_{18}$ Ring and from the Ring to the PSI_3 Core. Based on the arguments presented in Section 4.5, there are most likely three entry points for EET from the $IsiA_{18}$ ring to the PSI_3 core per PSI core monomer in our samples, with two entry points located on adjacent monomers; see Figure 14F (i.e., nine entry points per PSI_3 trimer). These data are consistent with the relatively large coupling constants between low energy IsiA 514, 517, and 511 Chls and PSI Chls close to the ring. Namely, the largest coupling constants are between Chls B32-n514 (40.8 cm^{-1}) and Chl B31-n514 (11 cm^{-1}). Chls A2, A8, A13, and A14 have also a relatively strong coupling to Chls q517, r517, and q511 (about 10−15 cm^{-1}). The yellow arrows in Figure 15 indicate likely excitation entry points from the hexamer to the PSI monomer. The shortest distances between IsiA Chls and PSI Chls (up to 20 Å) are shown in Figure S6 in the Supporting Information. Based on the coupling constants, the thicker the arrow the more likely EET is from the hexamer to the PSI monomer. The major entry point for EET to each PSI monomer is the B31−B32 dimer, which is one of the PSI_3 core low-energy traps (referred in the literature as the C706 trap).[25,58] However, some scenarios with two separate entry points (see Figure 14D) also cannot be excluded. In the latter case, we obtained a better match in terms of the emission peak wavelength but poorer match in terms of integral intensity of the emission. Three well-separated entry points or more than three entry points per PSI monomer would result in too little $IsiA_{18}$ ring emission compared to our data shown in Figure 3, while one entry point per PSI core monomer would result in too much IsiA ring emission (rendering the addition of the IsiA ring antenna nearly pointless). Estimated emission of the ring is in good agreement with the experiment and is less red-shifted than follows from just finding the lowest exciton state of the full set or six IsiA monomers (i.e., the hexamer). On the other hand, it is more red-shifted than the emission of the isolated intact monomers in agreement with data presented is Section 4.3. Integral intensity of the ring emission of around 10% of total supercomplex emission and smaller red shift (as observed in some earlier works)[15,30] imply three separate EET entry points, evenly distributed, or more than three entry points per PSI monomer, so there is never more than one inter-IsiA EET step before EET to the PSI core. Our current sample appears to have lower ring-core EET probability than those earlier samples. One can speculate that disruption of one entry

https://doi.org/10.1021/acs.jpcb.2c04829
J. Phys. Chem. B 2022, 126, 6891−6910

point and increased intensity of the red region of the PSI core might be related. Indeed, increased coupling between core pigments can cause both the shifts of the core excitonic states and the redistribution of their oscillator strength. Small shift of the core acceptor states/pigments (especially the blue shift that can render potential acceptors useless as opposed to just decreasing the spectral overlaps) could cause significant change of the EET effectiveness through one of the entry points.

Note that in Figure 14 it is implicitly assumed that EET out of the type-1 monomer is equally likely in both CW and CCW directions. This may not be the case. However, the exact proportion is difficult to estimate, as one has to take into account both the number and the availability of the acceptors in the CW and CCW directions. For instance, CW Chl 514 → 517 EET may outcompete all other EET processes, but many Chls 514 may not have available Chls 517 acceptors to the right, as those may absorb at higher energy. Results presented in Figure S5 indicate that slightly better agreement between simulations and the experiment is obtained in the case where excitations travel around the ring preferentially clockwise. In reality, the preferential direction of excitation travel along the ring (which could be modified with respect to what is shown in Figure 14 by introducing the uneven split of excitations exiting type-1 monomer) can originate from the differences between IsiA monomers in different locations with respect to the PSI core, resulting in slight shifts of the initial distributions of the oscillator strength of particular Chls such as those shown in Figure 12A. As can be seen from Tables S3−S8, structural differences between adjacent IsiA monomers in the ring are sufficient to result in significant changes in interpigment couplings for the same pairs of Chls. Thus, it is reasonable to expect a correlation between Chl site energies and the location of the IsiA monomer with respect to the PSI core (see insets in Figures 11 and S4).

6. CONCLUSIONS

Modeling of various optical spectra reported in this work is based on the structure of the PSI_3−$IsiA_{18}$ supercomplex from *Synechocystis sp.* PCC 6803 recently determined via cryo-EM imaging.[12] Two additional medium resolution structures of this supercomplex from different cyanobacteria have also been reported (2.9−3.48 Å).[23,32] Despite the lability of the complexes and the cofactors, all structures are highly similar and agree on the number of Chls (17) and carotenes (4) in individual IsiA monomer subunits. One discrepancy is the orientation of Chl 503, which is rotated 180° between the *Synechocystis sp.* PCC 6803 structure and the structure from *Synechococcus* PCC 7942 (Chl 513 in 6KIG).[23] Interestingly, both orientations can be fitted to the *Synechocystis* experimental cryo-EM map (data not shown). At this point, we cannot say which orientation is correct in *Synechocystis.* However, the change in orientation of Chl 503 does not affect our analysis, as both orientations can fit our absorption, emission, HB and CD spectra equally well provided a small adjustment of Chls site energies are made. Moreover, the change in orientation has a negligible effect on EET dynamics, as Chl 503 is definitely not one of the lower-energy pigments.

Based on the modeling results presented in this work we conclude that there are most likely three entry points for EET from the $IsiA_6$ hexamer to the PSI core monomer in our samples, with two of these entry points likely being located next to each other (i.e., nine entry points from $IsiA_{18}$ to the PSI_3 trimer). However, some scenarios with two separated entry points per PSI monomer cannot be excluded. Three well-separated entry points per PSI monomer could be present in the samples studied by other groups as suggested by some emission spectra reported in the literature.[15,17] Since the $IsiA_{18}$ ring can also act as an energy dissipater (to protect photosystems from being damaged by excess excitation energy),[26,27] it is feasible that bacteria described in the literature not all were grown under identical conditions (e.g., the same amount of light exposure) and developed somewhat different dissipation pathways. The latter could modify emission spectra from the $IsiA_{18}$ ring; i.e., a different number of entry points could be a genuine feature related to adaptation and a need to dissipate more energy before it gets to the reaction center. Thus, one could speculate that a different number or arrangement of connecting points from the $IsiA_{18}$ ring to the PSI_3 core could reflect adaptation to different light conditions. This could be studied in future experiments by growing bacteria at different light conditions. Nevertheless, we suggest that our samples have nine entry points from $IsiA_{18}$ to the PSI_3 trimer, with the best entry point for each PSI monomer likely being the C706 trap assigned in ref 25 to the B31−B32 dimer (see Figure 1).

Summarizing, multiple low-temperature spectra reported in this work for $IsiA_6$ hexamer are best described within model *HexB*, in which the lowest energy pigments are assigned to Chl 511 (a.k.a. Chl 44 assigned previously to state A′), 514 (a.k.a. Chl 37 previously assigned to state B′),[30] and the newly discovered Chl 517. In the model *HexB*, E_o/fwhm values for Chls 508 and 517 (missing in isolated monomers) are (14991/106 cm^{-1}) and (14770/185 cm^{-1}), respectively. E_o/fwhm values for Chl 511 (partly lost in isolated monomers) are 14717/61 cm^{-1}. We hasten to add that very similar calculated spectra were obtained for all three hexamers, as well as the entire $IsiA_{18}$ ring. Regarding the isolated monomers we showed that model *MB* is in very good agreement with the experimental data, implying that about 2.7 Chls are absent in the individual isolated IsiA complexes. The latter is consistent with the observed blue-shifted monomer emission in comparison with the red-shifted $IsiA_{18}$ ring emission (686 nm) and sample dependent maxima of single monomer fluorescence spectra (varying from 682 to 685 nm), as reported in the literature.[15,30] Although models *MA* and *MB* describe the absorption, emission and transient HB spectra well, model *MB* (assuming the absence of Chls 508/517 and 70% loss of Chl 511) provides a better match to the CD spectrum and observed EET dynamics. In model *HexB* describing $IsiA_6$ hexamers the values E_0/Γ_{inh} of Chl 514 (a.k.a. Chl 37), and Chl 511 (a.k.a. Chl 44) are 14713/153 cm^{-1} and 14717/61 cm^{-1}, respectively. That is, nearly identical site energies of Chls 514 and 511 and reversed extent of their inhomogeneities, in comparison to our previous works,[30] provided the best fit of multiple spectra, including a reasonable match to CD spectra from ref 15. Current modeling reveals that Chl 511 (i.e., Chl 44) has a smaller inhomogeneity (by a factor of 2.5) than Chl 514 (i.e., Chl 37). The lowest-energy Chl 514 (in monomers n, W, and t) with large inhomogeneous broadening has also the shortest distance between IsiA Chls and PSI red Chls (i.e., B31−B32 dimer, referred in our previous papers as the C706 trap).[25,58] This clearly indicates that at least three energy flows from the ring to PSI_3 core likely occur from monomers n, W, and t to the C706 traps (and subsequently to the C714 traps).[25] This was expected as the separation between Chls 514−517 in n−h, W−y, and v−t monomers are larger (~17 Å)

https://doi.org/10.1021/acs.jpcb.2c04829
J. Phys. Chem. B 2022, 126, 6891−6910

than separations between the same Chls in hexamer monomers (13.8−14.5 Å).

■ ASSOCIATED CONTENT

Supporting Information

The Supporting Information is available free of charge at https://pubs.acs.org/doi/10.1021/acs.jpcb.2c04829.

SDS-PAGE gel data; Chls numbering in the different PDB models reported in the literature; comment on the applicability of V_{nm} parameters calculated in the absence of Hydrogens for planar Chl molecules; coupling matrix elements (V_{nm}, in cm^{-1}) for various monomers; averaged site-energies (E_n^0) and Γ_{inh} of intact monomers within the $IsiA_{18}$ ring for models *HexA* and *HexB* (in cm^{-1}); averaged exciton energies with standard deviations (in cm^{-1}) for IsiA isolated monomers for 15 and 14 Chl present (based on models *MA* and MB; site energies and Γ_{inh} of 17 Chls averaged over all 18 subunits of the supercomplex ring for model *MA;* contributions ($|C_{mM}|^2$, in %) of fully occupied IsiA monomer "*n*" pigments *m* to excitonic states *M* calculated using models *HexA* and *HexB*; SDF serving as the origin of IsiA ring emission in model *HexB*; a figure showing the shortest distances between IsiA Chls and PSI Chls (up to 20 Å; view from the lumen side); comparison of excitonic structures of isolated IsiA monomers and intact monomers within the supercomplex ring; and definition of a transient hole (PDF)

■ AUTHOR INFORMATION

Corresponding Author

Ryszard Jankowiak − *Department of Chemistry and Department of Physics, Kansas State University, Manhattan, Kansas 66506, United States;* orcid.org/0000-0003-3302-9232; Email: ryszard@ksu.edu

Authors

Tonu Reinot − *Department of Chemistry, Kansas State University, Manhattan, Kansas 66506, United States;* Present Address: 13025 Morehead, Chapel Hill, NC 27517. Email: tonu.reinot@gmail.com

Anton Khmelnitskiy − *Department of Physics, Kansas State University, Manhattan, Kansas 66506, United States*

Valter Zazubovich − *Department of Physics, Concordia University, Montreal H4B 1R6, Canada;* orcid.org/0000-0001-7129-8391

Hila Toporik − *School of Molecular Sciences and Biodesign Center for Applied Structural Discovery, Arizona State University, Tempe, Arizona 85287, United States*

Yuval Mazor − *School of Molecular Sciences and Biodesign Center for Applied Structural Discovery, Arizona State University, Tempe, Arizona 85287, United States*

Complete contact information is available at: https://pubs.acs.org/10.1021/acs.jpcb.2c04829

Notes

The authors declare no competing financial interest.

■ ACKNOWLEDGMENTS

This work was supported by the U.S. Department of Energy, Office of Science, Office of Basic Energy Sciences, under Award Number DE-SC-0006678 (to R.J.). Work at Concordia University (V.Z.) was supported by NSERC. The data that support the findings of this study are available from the corresponding author upon a reasonable request.

■ REFERENCES

(1) Blankenship, R. E. *Molecular Mechanisms of Photosynthesis*; Wiley-Blackwell: 2002.

(2) Shevela, D.; Björn, L. O.; Govindjee *Photosynthesis*; World Scientific: 2018.

(3) Flombaum, P.; Gallegos, J. L.; Gordillo, R. A.; Rincon, J.; Zabala, L. L.; Jiao, N.; Karl, D. M.; Li, W. K. W.; Lomas, M. W.; Veneziano, D.; Vera, C. S.; Vrugt, J. A.; Martiny, A. C. Present and Future Global Distributions of the Marine Cyanobacteria *Prochlorococcus* and *Synechococcus*. *Proc. Natl. Acad. Sci. U. S. A.* **2013**, *110*, 9824−9829.

(4) Liu, H.; Nolla, H.; Campbell, L. Prochlorococcus Growth Rate and Contribution to Primary Production in the Equatorial and Subtropical North Pacific Ocean. *Aquatic Microbial Ecology* **1997**, *12*, 39−47.

(5) Field, C. B.; Behrenfeld, M. J.; Randerson, J. T.; Falkowski, P. Primary Production of the Biosphere: Integrating Terrestrial and Oceanic Components. *Science* **1998**, *281*, 237−240.

(6) Grossman, A. R.; Schaefer, M. R.; Chiang, G. G.; Collier, J. L. The Responses of Cyanobacteria to Environmental Conditions: Light and Nutrients. In *The Molecular Biology of Cyanobacteria*; Springer Netherlands: Dordrecht, The Netherlands, 1994; pp 641−675.

(7) González, A.; Fillat, M. F.; Bes, M.-T.; Peleato, M.-L.; Sevilla, E. The Challenge of Iron Stress in Cyanobacteria. In *Cyanobacteria*; InTech: 2018.

(8) Straus, N. A. Iron Deprivation: Physiology and Gene Regulation. In *The Molecular Biology of Cyanobacteria*; Springer Netherlands: Dordrecht, The Netherlands, 1994; pp 731−750.

(9) Guikema, J. A.; Sherman, L. A. Chlorophyll-Protein Organization of Membranes from the Cyanobacterium Anacystis Nidulans. *Arch. Biochem. Biophys.* **1983**, *220*, 155−166.

(10) Burnap, R. L.; Troyan, T.; Sherman, L. A. The Highly Abundant Chlorophyll-Protein Complex of Iron-Deficient *Synechococcus* Sp. PCC7942 (CP43′) Is Encoded by the IsiA Gene. *Plant Physiology* **1993**, *103*, 893−902.

(11) Laudenbach, D. E.; Straus, N. A. Characterization of a Cyanobacterial Iron Stress-Induced Gene Similar to PsbC. *J. Bacteriol.* **1988**, *170*, 5018−5026.

(12) Toporik, H.; Li, J.; Williams, D.; Chiu, P. L.; Mazor, Y. The Structure of the Stress-Induced Photosystem I-IsiA Antenna Supercomplex. *Nature Structural and Molecular Biology* **2019**, *26*, 443−449.

(13) Boekema, E. J.; Hifney, A.; Yakushevska, A. E.; Piotrowski, M.; Keegstra, W.; Berry, S.; Michel, K.-P.; Pistorius, E. K.; Kruip, J. A Giant Chlorophyll-Protein Complex Induced by Iron Deficiency in Cyanobacteria. *Nature* **2001**, *412*, 745−748.

(14) Bibby, T. S.; Nield, J.; Barber, J. Three-Dimensional Model and Characterization of the Iron Stress-Induced CP43′-Photosystem I Supercomplex Isolated from the Cyanobacterium *Synechocystis* PCC 6803. *J. Biol. Chem.* **2001**, *276*, 43246−43252.

(15) Andrizhiyevskaya, E. G.; Schwabe, T. M. E.; Germano, M.; D'Haene, S.; Kruip, J.; van Grondelle, R.; Dekker, J. P. Spectroscopic Properties of PSI-IsiA Supercomplexes from the Cyanobacterium *Synechococcus* PCC 7942. *Biochimica et Biophysica Acta (BBA) - Bioenergetics* **2002**, *1556*, 265−272.

(16) Dang, N. C.; Zazubovich, V.; Reppert, M.; Neupane, B.; Picorel, R.; Seibert, M.; Jankowiak, R. The CP43 Proximal Antenna Complex of Higher Plant Photosystem II Revisited: Modeling and Hole Burning Study. I. *J. Phys. Chem. B* **2008**, *112*, 9921−9933.

(17) Melkozernov, A. N.; Bibby, T. S.; Lin, S.; Barber, J.; Blankenship, R. E. Time-Resolved Absorption and Emission Show That the CP43′ Antenna Ring of Iron-Stressed *Synechocystis* Sp. PCC6803 Is Efficiently Coupled to the Photosystem I Reaction Center Core. *Biochemistry* **2003**, *42*, 3893−3903.

(18) Riley, K. J.; Zazubovich, V.; Jankowiak, R. Frequency-Domain Spectroscopic Study of the PS I - CP43′ Supercomplex from the

Cyanobacterium *Synechocystis* PCC 6803 Grown under Iron Stress Conditions. *J. Phys. Chem. B* **2006**, *110*, 22436−22446.
(19) Sun, J.; Golbeck, J. H. The Presence of the IsiA-PSI Supercomplex Leads to Enhanced Photosystem I Electron Throughput in Iron-Starved Cells of *Synechococcus* Sp. PCC 7002. *J. Phys. Chem. B* **2015**, *119*, 13549−13559.
(20) Bibby, T. S.; Nield, J.; Partensky, F.; Barber, J. Antenna Ring around Photosystem I. *Nature* **2001**, *413*, 590−590.
(21) Kouřil, R.; Zygadlo, A.; Arteni, A. A.; de Wit, C. D.; Dekker, J. P.; Jensen, P. E.; Scheller, H. V.; Boekema, E. J. Structural Characterization of a Complex of Photosystem I and Light-Harvesting Complex II of *Arabidopsis Thaliana*. *Biochemistry* **2005**, *44*, 10935−10940.
(22) Aspinwall, C. L.; Sarcina, M.; Mullineaux, C. W. Phycobilisome Mobility in the Cyanobacterium *Synechococcus* Sp. PCC7942 Is Influenced by the Trimerisation of Photosystem I. *Photosynthesis Research* **2004**, *79*, 179−187.
(23) Cao, P.; Cao, D.; Si, L.; Su, X.; Tian, L.; Chang, W.; Liu, Z.; Zhang, X.; Li, M. Structural Basis for Energy and Electron Transfer of the Photosystem I-IsiA-Flavodoxin Supercomplex. *Nature Plants* **2020**, *6*, 167−176.
(24) Akita, F.; Nagao, R.; Kato, K.; Nakajima, Y.; Yokono, M.; Ueno, Y.; Suzuki, T.; Dohmae, N.; Shen, J.-R.; Akimoto, S.; Miyazaki, N. Structure of a Cyanobacterial Photosystem I Surrounded by Octadecameric IsiA Antenna Proteins. *Communications Biology* **2020**, *3*, 232.
(25) Khmelnitskiy, A.; Toporik, H.; Mazor, Y.; Jankowiak, R. On the Red Antenna States of Photosystem I Mutants from Cyanobacteria *Synechocystis* PCC 6803. *J. Phys. Chem. B* **2020**, *124*, 8504−8515.
(26) Sandström, S.; Park, Y.-I.; Öquist, G.; Gustafsson, P. CP43′, the IsiA Gene Product, Functions as an Excitation Energy Dissipator in the Cyanobacterium *Synechococcus* Sp. PCC 7942. *Photochem. Photobiol.* **2001**, *74*, 431−437.
(27) Ihalainen, J. A.; D'Haene, S.; Yeremenko, N.; van Roon, H.; Arteni, A. A.; Boekema, E. J.; van Grondelle, R.; Matthijs, H. C. P.; Dekker, J. P. Aggregates of the Chlorophyll-Binding Protein IsiA (CP43′) Dissipate Energy in Cyanobacteria. *Biochemistry* **2005**, *44*, 10846−10853.
(28) Havaux, M.; Guedeney, G.; Hagemann, M.; Yeremenko, N.; Matthijs, H. C. P.; Jeanjean, R. The Chlorophyll-Binding Protein IsiA Is Inducible by High Light and Protects the Cyanobacterium *Synechocystis* PCC6803 from Photooxidative Stress. *FEBS Lett.* **2005**, *579*, 2289−2293.
(29) Andrizhiyevskaya, E. G.; Frolov, D.; van Grondelle, R.; Dekker, J. P. On the Role of the CP47 Core Antenna in the Energy Transfer and Trapping Dynamics of Photosystem II. *Phys. Chem. Chem. Phys.* **2004**, *6*, 4810.
(30) Feng, X.; Neupane, B.; Acharya, K.; Zazubovich, V.; Picorel, R.; Seibert, M.; Jankowiak, R. Spectroscopic Study of the CP43′ Complex and the PSI-CP43′ Supercomplex of the Cyanobacterium *Synechocystis* PCC 6803. *J. Phys. Chem. B* **2011**, *115*, 13339−13349.
(31) Umena, Y.; Kawakami, K.; Shen, J.-R.; Kamiya, N. Crystal Structure of Oxygen-Evolving Photosystem II at a Resolution of 1.9 Å. *Nature* **2011**, *473*, 55−60.
(32) Zhang, Y.; Chen, M.; Church, W. B.; Lau, K. W.; Larkum, A. W. D.; Jermiin, L. S. The Molecular Structure of the IsiA-Photosystem I Supercomplex, Modelled from High-Resolution, Crystal Structures of Photosystem I and the CP43 Protein. *Biochimica et Biophysica Acta (BBA) - Bioenergetics* **2010**, *1797*, 457−465.
(33) Nield, J.; Morris, E. P.; Bibby, T. S.; Barber, J. Structural Analysis of the Photosystem I Supercomplex of Cyanobacteria Induced by Iron Deficiency. *Biochemistry* **2003**, *42*, 3180−3188.
(34) Jankowiak, R.; Reppert, M.; Zazubovich, V.; Pieper, J.; Reinot, T. Site Selective and Single Complex Laser-Based Spectroscopies: A Window on Excited State Electronic Structure, Excitation Energy Transfer, and Electron-Phonon Coupling of Selected Photosynthetic Complexes. *Chem. Rev.* **2011**, *111*, 4546−4598.
(35) Jankowiak, R.; Hayes, J. M.; Small, G. J. Spectral Hole-Burning Spectroscopy in Amorphous Molecular Solids and Proteins. *Chem. Rev.* **1993**, *93*, 1471−1502.
(36) Johnson, S. G.; Tang, D.; Jankowiak, R.; Hayes, J. M.; Small, G. J.; Tiede, D. M. Primary Donor State Mode Structure and Energy Transfer in Bacterial Reaction Centers. *J. Phys. Chem.* **1990**, *94*, 5849−5855.
(37) Shuvalov, V. A.; Klevanik, A. V.; Ganago, A. O.; Shkuropatov, A. Ya.; Gubanov, V. S. Burning of a Narrow Spectral Hole at 1.7 K in the Absorbance Band of the Primary Electron Donor of *Rhodopseudomonas viridis* Reaction Centers with Blocked Electron Transfer. *FEBS Lett.* **1988**, *237*, 57−60.
(38) Reddy, N. R. S.; Lyle, P. A.; Small, G. J. Applications of Spectral Hole Burning Spectroscopies to Antenna and Reaction Center Complexes. *Photosynthesis Research* **1992**, *31*, 167−194.
(39) Renger, T.; Marcus, R. A. On the Relation of Protein Dynamics and Exciton Relaxation in Pigment-Protein Complexes: An Estimation of the Spectral Density and a Theory for the Calculation of Optical Spectra. *J. Chem. Phys.* **2002**, *116*, 9997−10019.
(40) Madjet, M. E.; Abdurahman, A.; Renger, T. Intermolecular Coulomb Couplings from Ab Initio Electrostatic Potentials: Application to Optical Transitions of Strongly Coupled Pigments in Photosynthetic Antennae and Reaction Centers. *J. Phys. Chem. B* **2006**, *110*, 17268−17281.
(41) Müh, F.; Madjet, M. E. A.; Renger, T. Structure-Based Identification of Energy Sinks in Plant Light-Harvesting Complex II. *J. Phys. Chem. B* **2010**, *114*, 13517−13535.
(42) Adolphs, J.; Muh, F.; Madjet, M.; Schmidt am Busch, M.; Renger, T. Structure-Based Calc Optical Spectra of Photosystem I Suggest an Asymm Light-Harvesting Process. *J. Am. Chem. Soc.* **2010**, *132*, 3331−3343.
(43) Jassas, M.; Chen, J.; Khmelnitskiy, A.; Casazza, A. P.; Santabarbara, S.; Jankowiak, R. Structure-Based Exciton Hamiltonian and Dynamics for the Reconstituted Wild-Type CP29 Protein Antenna Complex of the Photosystem II. *J. Phys. Chem. B* **2018**, *122*, 4611−4624.
(44) Hall, J.; Renger, T.; Picorel, R.; Krausz, E. Circularly Polarized Luminescence Spectroscopy Reveals Low-Energy Excited States and Dynamic Localization of Vibronic Transitions in CP43. *Biochimica et Biophysica Acta (BBA) - Bioenergetics* **2016**, *1857*, 115−128.
(45) Zazubovich, V.; Jankowiak, R. How Well Does the Hole-Burning Action Spectrum Represent the Site-Distribution Function of the Lowest-Energy State in Photosynthetic Pigment-Protein Complexes? *J. Phys. Chem. B* **2019**, *123*, 6007−6013.
(46) Herascu, N.; Kell, A.; Acharya, K.; Jankowiak, R.; Blankenship, R. E.; Zazubovich, V. Modeling of Various Optical Spectra in the Presence of Slow Excitation Energy Transfer in Dimers and Trimers with Weak Interpigment Coupling: FMO as an Example. *J. Phys. Chem. B* **2014**, *118*, 2032−2040.
(47) Herascu, N.; Ahmouda, S.; Picorel, R.; Seibert, M.; Jankowiak, R.; Zazubovich, V. Effects of the Distributions of Energy or Charge Transfer Rates on Spectral Hole Burning in Pigment-Protein Complexes at Low Temperatures. *J. Phys. Chem. B* **2011**, *115*, 15098−15109.
(48) Jang, S.; Newton, M. D.; Silbey, R. J. Multichromophoric Förster Resonance Energy Transfer. *Phys. Rev. Lett.* **2004**, *92*, 218301.
(49) Scholes, G. D.; Fleming, G. R. On the Mechanism of Light Harvesting in Photosynthetic Purple Bacteria: B800 to B850 Energy Transfer. *J. Phys. Chem. B* **2000**, *104*, 1854−1868.
(50) Sumi, H. Theory on Rates of Excitation-Energy Transfer between Molecular Aggregates through Distributed Transition Dipoles with Application to the Antenna System in Bacterial Photosynthesis. *J. Phys. Chem. B* **1999**, *103*, 252−260.
(51) Reppert, M.; Zazubovich, V.; Dang, N. C.; Seibert, M.; Jankowiak, R. Low-Energy Chlorophyll States in the CP43 Antenna Protein Complex: Simulation of Various Optical Spectra. II. *J. Phys. Chem. B* **2008**, *112*, 9934−9947.
(52) Schlodder, E.; Lendzian, F.; Meyer, J.; Çetin, M.; Brecht, M.; Renger, T.; Karapetyan, N. V. Long-Wavelength Limit of Photo-

https://doi.org/10.1021/acs.jpcb.2c04829
J. Phys. Chem. B 2022, 126, 6891−6910

chemical Energy Conversion in Photosystem I. *J. Am. Chem. Soc.* **2014**, *136*, 3904−3918.
(53) Herascu, N.; Hunter, M. S.; Shafiei, G.; Najafi, M.; Johnson, T. W.; Fromme, P.; Zazubovich, V. Spectral Hole Burning in Cyanobacterial Photosystem I with P700 in Oxidized and Neutral States. *J. Phys. Chem. B* **2016**, *120*, 10483−10495.
(54) Zazubovich, V.; Jankowiak, R. On the Energy Transfer between Quasi-Degenerate States with Uncorrelated Site Distribution Functions: An Application to the CP43 Complex of Photosystem II. *J. Lumin.* **2007**, *127*, 245−250.
(55) Schlodder, E.; Falkenberg, K.; Gergeleit, M.; Brettel, K. Temperature Dependence of Forward and Reverse Electron Transfer from A1-, the Reduced Secondary Electron Acceptor in Photosystem I. *Biochemistry* **1998**, *37*, 9466−9476.
(56) Pålsson, L. O.; Flemming, C.; Gobets, B.; van Grondelle, R.; Dekker, J. P.; Schlodder, E. Energy Transfer and Charge Separation in Photosystem I: P700 Oxidation upon Selective Excitation of the Long-Wavelength Antenna Chlorophylls of *Synechococcus elongatus*. *Biophys. J.* **1998**, *74*, 2611−2622.
(57) Najafi, M.; Herascu, N.; Shafiei, G.; Picorel, R.; Zazubovich, V. Conformational Changes in Pigment-Protein Complexes at Low Temperatures—Spectral Memory and a Possibility of Cooperative Effects. *J. Phys. Chem. B* **2015**, *119*, 6930−6940.
(58) Riley, K. J.; Reinot, T.; Jankowiak, R.; Fromme, P.; Zazubovich, V. Red Antenna States of Photosystem I from Cyanobacteria Synechocystis PCC 6803 and Thermosynechococcus Elongatus: Single-Complex Spectroscopy and Spectral Hole-Burning Study. *J. Phys. Chem. B* **2007**, *111*, 286−292.

https://doi.org/10.1021/acs.jpcb.2c04829
J. Phys. Chem. B 2022, 126, 6891−6910